

AMERICAN UNIVERSITY OF BEIRUT

NUMERICAL SOLUTION OF THE POPULATION BALANCE
EQUATION UNDER TURBULENT FLOW CONDITIONS

by
SAKINA HICHAM TAKACHE

A thesis
submitted in partial fulfillment of the requirements
for the degree of Master of Sciences
to the Department of Computational Science
of the Faculty of Arts and Sciences
at the American University of Beirut

Beirut, Lebanon
May 2018

AMERICAN UNIVERSITY OF BEIRUT

NUMERICAL SOLUTION OF THE POPULATION BALANCE
EQUATION UNDER TURBULENT FLOW CONDITIONS

by
SAKINA HICHAM TAKACHE

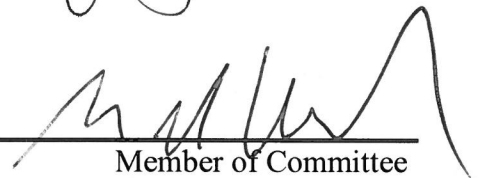
Approved by:

Dr. Fouad Azizi, Associate Professor
Department of Chemical and Petroleum Engineering



Adviser

Dr. Mazen Al Ghouli, Professor
Department of Chemistry



Member of Committee

Dr. Joseph Zeaiter, Associate Professor
Department of Chemical and Petroleum Engineering



Member of Committee

Date of thesis defense: May 9, 2018

AMERICAN UNIVERSITY OF BEIRUT

THESIS, DISSERTATION, PROJECT RELEASE FORM

Student Name:

Hicham

Takache

Sakina

Middle

Last

First

Master's Thesis

Master's Project

Doctoral Dissertation

I authorize the American University of Beirut to: (a) reproduce hard or electronic copies of my thesis, dissertation, or project; (b) include such copies in the archives and digital repositories of the University; and (c) make freely available such copies to third parties for research or educational purposes.

I authorize the American University of Beirut to: (a) reproduce hard or electronic copies of it; (b) include such copies in the archives and digital repositories of the University; and (c) make freely available such copies to third parties for research or educational purposes after:

one year from the date of submission of my thesis, dissertation, or project.

two years from the date of submission of my thesis, dissertation, or project.

three years from the date of submission of my thesis, dissertation, or project.


Signature

14-5-2018

Date

ACKNOWLEDGMENTS

Thanks are in order, first and foremost, to my enthusiastically and undyingly supportive parents, Fatima and Hicham Takache, to my technical support professional, catalyst and backbone, Ali Mokh, and to my very patient - and rather accurate - thesis adviser, Dr. Fouad Azizi.

Secondly, I thank my academic adviser who guided me through this degree both academically and professionally, Prof. Mazen Al Ghoul.

AN ABSTRACT OF THE THESIS OF

Sakina Hicham Takache for Master of Science
Major: Computational Science

Title: Numerical Solution for the Population Balance Equation under Turbulent Flow Conditions

In this work, the algorithm developed by Azizi and Al Taweel (2011) to solve the population balance equation using the sampling approach and the moving grid technique will be used to solve the population balance equation under various operating conditions. Two models will be employed to simulate turbulently flowing gas-liquid systems, namely, the models of Coualoglou and Tavlarides (1977), and Wang et al. (2003).

The models will be used to simulate the two-phase flow in pipes equipped with static mixers that exhibit regions of low, moderate, and high energy dissipation, where the conditions change drastically in very short times. The model constants used in the model of Coualoglou and Tavlarides (1977) will first be optimized. The simulation results will then be compared to experimental results for validation.

CONTENTS

ACKNOWLEDGMENTS	v
ILLUSTRATIONS	ix
TABLES	xi
NOTATIONS	xii
ABBREVIATIONS	xv
DEDICATION.....	v

Chapter

1. INTRODUCTION	1
2. LITERATURE REVIEW	8
2.1. Background	8
2.2. Advances in PB Modeling	10
2.2.1. <i>Advances in PB Modeling Applications</i>	10
2.2.2. <i>Advances in Methods of Solution</i>	10
2.2.3. <i>Kernel Development</i>	15
2.3. Gas-Liquid PB Applications	24
2.4. Liquid-Liquid PB Applications.....	27
3. MATHEMATICAL MODELING	30
3.1. Population Balance Equation	30
3.2. The Kernels of Coualaloglou and Tavlarides (1977).....	32
3.2.1. <i>Coalescence Terms</i>	32
3.2.2. <i>Breakage Terms</i>	34
3.3. The Kernels of Wang et al. (2003, 2005a).....	36
3.3.1. <i>Coalescence Terms</i>	36
3.3.2. <i>Breakage Terms</i>	40

4. NUMERICAL SOLUTION AND RESULTS	45
4.1. Numerical Solution of PBE and Coefficient Optimization.....	45
4.1.1. <i>Solution Methodology</i>	45
4.2. Results and Validation	56
4.2.1. <i>Numerical Findings on the Optimization of Coefficients</i>	56
4.2.2. <i>Wang Model</i>	65
4.3. <i>Discussion</i>	73
5. CONCLUSION AND RECOMMENDATIONS	75
5.1. Conclusion.....	75
5.1.1. <i>Optimization of Coefficients</i>	75
5.1.2. <i>Wang et al. (2003, 2005a) Model Implementation</i>	76
5.2. Recommendations	78
5.2.1. <i>Optimization of Coefficients</i>	78
5.2.2. <i>Wang et al. (2003, 2005a) Model Implementation</i>	79
REFERENCES	81

ILLUSTRATIONS

Figure		Page
1	Overall algorithm for solving the PBE	47
2	The spatial variation of the calculated Sauter mean diameter along the reactor/contact length ($U=1.3$ m/s, $\Phi=7\%$, $C_{SDS}=0$ ppm) with the corresponding experimentally measured values of the Sauter mean diameter	57
3	The spatial variation of the calculated Sauter mean diameter along the reactor/contact length ($U=2$ m/s, $\Phi=7\%$, $C_{SDS}=0$ ppm) with the corresponding experimentally measured values of the Sauter mean diameter	57
4	The spatial variation of the calculated sauter mean diameter along the reactor/contact length ($U=2.3$ m/s, $\Phi=7\%$, $C_{SDS}=0$ ppm) with the corresponding experimentally measured values of the Sauter mean diameter	58
5	The spatial variation of the calculated Sauter mean diameter along the reactor/contact length ($U=2$ m/s, $\Phi=7\%$, $C_{SDS}=2$ ppm) with the corresponding experimentally measured values of the Sauter mean diameter	60
6	The spatial variation of the calculated Sauter mean diameter along the reactor/contact length ($U=2$ m/s, $\Phi=7\%$, $C_{SDS}=5$ ppm) with the corresponding experimentally measured values of the Sauter mean diameter	61
7	The spatial variation of the calculated Sauter mean diameter along the reactor/contact length ($U=2$ m/s, $\Phi=7\%$, $C_{SDS}=10$ ppm) with the experimentally measured values of the Sauter mean diameter	62
8	Effect of SDS concentration on the average Sauter mean diameter in stage 6 (35 cm to 42 cm range) of the pipe	63
9	Effect of Varying the Superficial Velocity and Holdup on the Equilibrium Sauter Mean Diameter in Stage 6	64
10	Typical curves for the birth by coalescence rate at typical diameter values in the system for energy dissipation rates of $10\text{ m}^2\text{s}^{-3}$, $100\text{ m}^2\text{s}^{-3}$, $1000\text{ m}^2\text{s}^{-3}$, and $4000\text{ m}^2\text{s}^{-3}$	66

11	Typical curves for the death by coalescence rate at typical diameter values in the system for energy dissipation rates of $10 \text{ m}^2\text{s}^{-3}$, $100 \text{ m}^2\text{s}^{-3}$, $1000 \text{ m}^2\text{s}^{-3}$, and $4000 \text{ m}^2\text{s}^{-3}$	67
12	The birth by coalescence rates (positive) and the death by coalescence rates (negative) for typical diameter values in the system at energy dissipation rates of $10 \text{ m}^2\text{s}^{-3}$, $100 \text{ m}^2\text{s}^{-3}$, $1000 \text{ m}^2\text{s}^{-3}$, and $4000 \text{ m}^2\text{s}^{-3}$	68
13	Typical curves for birth by breakage rate at typical diameters in the system for energy dissipation rates of $100 \text{ m}^2\text{s}^{-3}$, $1000 \text{ m}^2\text{s}^{-3}$, and $4000 \text{ m}^2\text{s}^{-3}$	69
14	The breakage frequency (a) and the corresponding death by breakage rate (b) over the diameter sample points for a twice-as-fine discretization of the energy domain	70
15	The breakage frequency (a) and the corresponding death by breakage rate (b) over the diameter sample points for a fifty-fold discretization of the energy domain	71
16	The overall solution of the PBE at reduced energy dissipation along the pipe	72
17	The overall solution of the PBE at 50-fold discretization of the energy domain	73

TABLES

Table		Page
1	Optimized values of the breakage and coalescence parameters for surfactant concentrations $C_{\text{SDS}} = 0$ ppm, $C_{\text{SDS}} = 2$ ppm, $C_{\text{SDS}} = 5$ ppm, $C_{\text{SDS}} = 10$ ppm	56

NOTATIONS

$A(d_j, t)$	probability density of a bubble of diameter d_j at a time t , $\text{m}^{-3}\text{s}^{-1}$
$b(f_v d)$	breakage rate of a bubble of diameter d breaking with breakup fraction f_v
B_b	birth rate by breakage per unit volume, $\text{m}^{-3}\text{s}^{-1}$
B_c	birth rate by coalescence per unit volume, $\text{m}^{-3}\text{s}^{-1}$
d	diameter, m
d_b	size of turbulent eddy, m
D_b	death rate by breakage per unit volume, $\text{m}^{-3}\text{s}^{-1}$
D_c	death rate by coalescence per unit volume, $\text{m}^{-3}\text{s}^{-1}$
$e(\lambda)$	eddy energy, J
$\bar{e}(\lambda)$	mean kinetic energy of the eddies, J
$e(\lambda)_{\text{cutoff}}$	maximum eddy energy, J
$e(\lambda)_{\text{min}}$	minimum eddy energy, J
f_v	breakup fraction, dimensionless
f_{vc}	critical breakup fraction, dimensionless
$f_{v,\text{max}}$	maximum breakage fraction, dimensionless
$f_{v,\text{min}}$	minimum breakage fraction, dimensionless
$g(d_i)$	breakage frequency of bubbles of diameter d_i , s^{-1}
$h_{b,ij}$	distance coefficient between bubbles of sizes d_j and d_i , m
$h_c(d_j, d_i)$	collision frequency between drops/bubbles of sizes d_j and d_i , s^{-1}
k	proportionality factor, $\text{m}^{-1/3}$
l_{bt}	individual turbulent path length, m

$l_{bt,ij}$	mean relative turbulent path length of drops of sizes d_i and d_j , m
n_i	number density of bubbles, m^{-4}
n_λ	number density of eddies of size λ , m^{-4}
$N(t)$	total number of bubbles in the system, dimensionless
N_i	number of bubbles of size d_i in i^{th} bubble region, m^{-3}
$P_b(f_v d, \lambda)$	breakup probability density for a bubble of size d of breaking fraction f_v hit by an eddy of size λ , dimensionless
$P_b(f_v d, e(\lambda), \lambda)$	probability of a droplet of size d breaking with breakup fraction f_v , dimensionless
$P_e(e(\lambda))$	energy distribution of eddies of size λ , J^{-1}
t	time, s
t_{ij}	coalescence time between bubbles of sizes d_i and d_j , s
\bar{u}_{bt}	mean speed of turbulent eddy, m/s
\bar{u}_i	mean speed of bubble of size d_i , m/s
\bar{u}_{ij}	mean-square root of the colliding bubble velocities, m/s
\bar{u}_λ	mean speed of eddies of size λ , m/s
$v(d_i)$	number of dispersed fluid entities formed from the breakage of bubbles of size d_i , dimensionless
We_{ij}	Weber number, dimensionless

Greek Letters

$\beta(d_i, d_j)$	size distribution of daughter drops/bubbles formed from the breakage of a drop/bubble of size d_i , dimensionless
γ	virtual mass coefficient, dimensionless

Γ_{ij}	coefficient related to bubble distance, dimensionless
δ	denominator threshold, dimensionless
Δd_i	diameter increment in the i th bubble size region, m
ε	energy dissipation rate, m^2s^{-3}
λ	eddy size, m
$\lambda_c(d_j, d_i)$	coalescence efficiency between drops/bubbles of sizes d_j and d_i , dimensionless
λ_{\min}	minimum eddy size effective for bubble breakup, m
μ_c	dynamic viscosity of the continuous phase, $\text{kg m}^{-1}\text{s}^{-1}$
ξ_{ij}	ratio of bubble/drop diameters, dimensionless
ρ_c	continuous phase density, kg m^{-3}
ρ_d	dispersed phase density, kg m^{-3}
σ	Static surface tension, N m^{-1}
τ_e	lifetime of turbulent eddy, s
τ_{ij}	contact time between bubbles of sizes d_i and d_j , s
Φ_d	dispersed phase volume fraction, dimensionless
$\Phi_{d,\max}$	maximum possible dispersed phase volume fraction, dimensionless
ψ	model parameter of order unity, dimensionless

ABBREVIATIONS

BIT	Bubble-Induced Turbulence
BSD	Bubble Size Distribution
CFD	Computational Fluid Dynamics
CQMOM	Conditional Quadrature Method of Moments
CSDS	Concentration of Sodium Dodecyl Sulfate
DPBE	Discretized Population Balance Equation
DSD	Drop Size Distribution
MC	Monte Carlo
PB	Population Balance
PBE	Population Balance Equation
PBM	Population Balance Modeling
PDF	Probability Density Function
PIV	Particle Image Velocimetry
ppm	Parts Per Million
PVC	Poly-Vinyl Chloride
QBMM	Quadrature-Based Methods of Moment

QMOM	Quadrature Method of Moments
RDC	Rotating-Disc Contactor
SDS	Sodium Dodecyl Sulfate

DEDICATION

*To those who gave their lives so that we may have ours and live them more abundantly;
to the martyrs of AUB, of whom I mention Ali Sadeq (1988), Hilal Alawiyyeh (2006),
Muhammad Jouni (2015), Hussein Assaad (2017), and those who await their turn.*

CHAPTER 1

INTRODUCTION

Multiphase flow phenomena play an important role in the chemical and process industries. These processes include unit operations carried out in batch and continuous stirred tanks, bubble and liquid-liquid extraction columns, airlift reactors, and many others. Designing those units is still very difficult without recourse to empiricism (e.g. pilot plants) which may not be applied with confidence beyond the specific range of operating conditions and geometries over which the relations were determined (Joshi, 2002). The use of empirical correlations is also limited due to the fact that oversimplifications are associated with their development, rendering them inapplicable to many practical situations without the incorporation of inefficient safety margins (Jonsson and Palsson, 1991). Consequently, most multiphase contactors/reactors presently used are inefficiently designed with subsequent adverse effects on the reaction yield and selectivity, and possibly on the mass transfer performance (Azizi and Al Taweel, 2011).

These hydrodynamic non-uniformities are largely reduced when conventional mixers are replaced by static mixers. These mixers consist of a series of motionless inserts installed in pipes or transfer tubes whose purpose is to better homogenize the flow while being transported (Rauline et al., 1998, 2000). Static mixers present an attractive alternative to conventional agitation methods (e.g. stirred tanks, bubble columns, mechanically agitated tanks, etc.) due to their inherent advantages whereby similar or better performance can be achieved at lower capital and operating costs

(Thakur et al., 2003; Ghanem et al., 2014). A large number of static mixers is commercially available, each presenting a different geometry and mixing approach. Screen-type static mixers are one variant which is used to repetitively superimpose an adjustable uniformly distributed turbulence field on the nearly plug flow conditions encountered in high velocity pipe flows, making them particularly effective in processing multiphase systems (Al Taweel and Chen, 1996; Azizi and Al Taweel, 2007). The very high turbulence intensities generated downstream of the screens result in the formation of fine dispersed phase bubbles/drops, which consequently enhance the value of the inter-phase mass transfer coefficient (Al Taweel et al., 2005, 2007; Azizi and Al Taweel, 2015). The relatively uniform energy dissipation rates prevalent in the downstream regions behind screens offer ideal conditions for investigating bubble/drop breakage and coalescence under turbulent conditions, and the assessment of the models proposed for such processes (Azizi and Al Taweel, 2007, 2010, 2011). Additionally, screens were found to reduce axial dispersions in the flow, thereby approaching plug flow conditions which are favorable in designing tubular chemical reactors (Ziókowski and Morawski, 1987; Hweij and Azizi, 2015; Azizi and Abou Hweij, 2017). Screen-type static mixers were also found to promote contact between immiscible fluids five times more efficiently than mechanically agitated tanks equipped with Rushton-type impellers (Al Taweel and Chen, 1996). This factor, combined with the high inter-phase mass transfer coefficients, resulted in volumetric mass transfer coefficients as high as 13 s^{-1} for liquid-liquid dispersions, enabling 99% of equilibrium conditions to be attained in less than 1s (Al Taweel et al., 2007). Similarly, for gas-liquid contacting, the use of multistage screen-type contactors resulted in interfacial areas as high as $2700 \text{ m}^2/\text{m}^3$ (Chen and Al Taweel, 2007). Also, oxygen-transfer efficiencies as high as

4.2 kg/kWh were achieved even in the presence of surfactants (Al Taweel et al., 2005), and volumetric mass transfer coefficients as high as 4.1 s^{-1} were also measured (Azizi and Al Taweel, 2015). Furthermore, screens have long been used to produce or reduce turbulence scales and intensities, and to create or remove mean velocity non-uniformities (Oshinowo and Kuhn, 2000). Inasmuch, the quasi-isotropic turbulence generated by the screens was used to study the effect of turbulent mixing on the evolution of chemical reactions (Bennani et al., 1985), and served as a medium for testing the applicability of micro-mixing models (Bourne and Lips, 1991).

Since the hydrodynamic conditions prevailing in pipes equipped with screen-type static mixers closely approach those of isotropic homogeneous turbulence with alternating breakage-dominated and coalescence-dominated regions, they offer a pseudo-ideal situation to test the various models proposed in the literature and validate simulation results. Furthermore, drop/bubble breakage and coalescence kernels, in addition to mass transfer models, identified in such geometries are expected to apply to other more complex hydrodynamic conditions (such as those encountered in mechanically-agitated tanks) provided that information about the local energy dissipation and velocity streamlines is available.

The complex, non-linear, interaction of the various mechanisms involved in multiphase mixing processes renders impossible the proposition of scale-up and design rules of contactors/reactors from experimental data (Marchisio et al., 2003). The design of these contactors/reactors thus requires not only a knowledge of the dynamic properties of the dispersion, such as drop/bubble size distributions and residence time, but also the dynamic rate characteristics of drop/bubble breakage and coalescence. Hence, better understanding of the factors governing the evolution of drop/bubble size,

the interfacial area of contact, and the mass transfer coefficient in turbulent systems is an area of major interest because of its ability to generate rational and acceptable design and scale-up methodologies for multiphase contactors/reactors. This can thus help in optimizing the performance, economy, and safety of these industrial systems. To achieve such a goal, mathematical models capable of accurately predicting drop size and motion within the contactor/reactor in question (including drop breakage and coalescence), as well as the mass transfer coefficient within the contactor, are needed. This necessitates the use of the population balance equation (PBE) which can be used to handle bubble breakage and coalescence within various regions of the contactor, and the identification of the breakage/coalescence kernels that can accurately describe these processes.

A detailed description of the dispersed phase characteristics can be obtained by using the population balance models introduced in 1964 (Hulbert and Katz, 1964; Randolph, 1964), to simulate chemical engineering operations. PBEs have since become a well-established tool that is widely used for simulating dispersed phase operations, because they have the advantage of being able to describe drop/bubble breakage and coalescence processes in terms of identifiable physical parameters and operational conditions (Argyriou et al., 1971; Coualoglou and Tavlarides, 1977; Ramkrishna, 1985; Guido-Lavalle et al., 1994; Tsouris and Tavlarides, 1994; Herrero et al., 1995; Kocamustafaogullari and Ishii, 1995; Millies and Mewes, 1999; Rigopoulos, 2010; Ekambara et al., 2012; Kálal et al., 2014; Rao et al., 2016). The biggest uncertainty associated with the use of PBEs to simulate multi-phase fluid processing (i.e. immiscible liquid-liquid and gas-liquid system) remains the identification of the breakage and coalescence kernels that most accurately describe what happens in

turbulent flows (Azizi and Al Taweel, 2010). Most of the models developed over the past several decades were verified using experimental data obtained in mechanically agitated tanks in which the dispersed phase holdup, drop size distribution, and energy dissipation rate are inaccurately assumed to be uniformly distributed throughout the volume of the mixing vessel. The fact that such units exhibit a broad residence time distribution, and that drops periodically circulate between the regions of high and low energy dissipation rates present in the mixing tank where the local energy dissipation rates can vary by a factor of 10,000 (Kumar, 2009; Azizi and Al Taweel, 2010), renders these assumptions erroneous to an extent. Unfortunately, while simulating multiphase systems using PBEs, little attention was given to the sources of error arising from improper modeling of the hydrodynamic situation, such as the assumption that the energy dissipation rate is uniform throughout the vessel (Wang et al., 2005b). However, computational fluid dynamics (CFD) has now become a standard tool in simulating the hydrodynamics of any reactor/contacter. Its ability to provide accurate information about flow hydrodynamics in complex geometries renders it a popular tool to be used in conjunction with the PBE (Harris et al., 1996; Sahu et al., 1999; Alopaeus et al., 1999; Sommerfeld and Decker, 2004; Ekambara et al., 2012; Amokrane et al., 2014). With the continuous improvements and availability of large computational facilities, results with increasing accuracy can be obtained using more advanced turbulence models (Brucato et al., 2000; Ekambara et al., 2012). However, the ultimate success of this approach remains the ability of PBEs to yield realistic and accurate descriptions of the overall drop breakage/coalescence processes.

Another factor which limited the widespread use of PBEs is the difficulty to obtain accurate solutions as the analytical solutions are rare and include major

simplifying assumptions that may not be met in practice. PBEs are complex integro-differential equations that are solved much more easily using numerical methods. For this purpose, a multitude of numerical solution methods has been employed, though each one renders a different accuracy and has its own shortfalls. These methods include the method of moments (Hulburt and Katz, 1964), the stochastic Monte Carlo method (Spielman and Levenspiel, 1965), the finite difference or discretization method (Batterham et al., 1981), the fixed pivot method (Kumar and Ramkrishna, 1996a), the Galerkin method (Galerkin, 1915) and many others. Starting with the work of Valentas and Amundson (1966), and followed by Kumar and Ramkrishna (1996a, b) and Balliu et al. (2004), the method of discretization of the continuous PBE emerged as an attractive alternative to other numerical methods of solution, and has been successfully used to provide accurate numerical solutions of the PBE (Chen et al., 2005a, b; Schmidt et al., 2006; Azizi and Al Taweel, 2007; Podila et al., 2007; Laakkonen et al., 2007).

In 2002, Al Taweel et al. proposed an algorithm to solve the PBE by the method of discretization based on the reduction of the error which usually results from discretizing the drop size domain, while maintaining the optimum drop size ranges for integration. This algorithm was employed successfully in 2005 then 2007 by Azizi and Al Taweel to describe multiphase operations, but the solution remained unstable for high shear conditions. This was attributed to the very high breakage and coalescence frequencies that are expected to dominate in such regions, causing a divergent solution to be encountered in many cases. Azizi and Al Taweel (2010) then used the size distribution sampling approach combined with a moving grid technique to improve their earlier work. In addition, they proposed an enhanced solution stability algorithm, which relies on monitoring the onset of errors in the various birth and death terms encountered

in the PBE. This approach allowed for corrective action to be undertaken before the errors would propagate in an uncontrollable fashion, and was found to improve the stability and robustness of the solution method even under very high shear-rate conditions. The authors later employed their algorithm to successfully simulate liquid-liquid flows in tubular reactors equipped with screen-type static mixers (Azizi and Al Taweel, 2011).

The objective of this work is therefore to employ the algorithm developed by Azizi and Al Taweel (2011) to simulate a two-phase turbulent gas-liquid flow in pipes equipped with static mixers. The simulation results will be validated against experimental measurements while using the model of Coualoglou and Tavlarides (1977) at first. Secondly, the breakage and coalescence models of Wang et al. (2003) will be incorporated into the solution algorithm and used instead of the kernels of Coualoglou and Tavlarides to simulate the system. The models of Wang et al. offer the advantage of not having any adjustable parameters, while providing better interpretation of the hydrodynamic effects on the breakage and coalescence of dispersed phase entities.

CHAPTER 2

LITERATURE REVIEW

2.1. Background

The population balance (PB) approach is used for the description of drop/bubble/particle dynamics in flow fields with various aspects. This method is significantly advantageous because it allows the inclusion of the details of the breakage and coalescence processes in terms of identifiable physical parameters and operational conditions. The solved PBE allows the prediction of the instantaneous drop size distribution (DSD), which in turn allows the detailed description of the hydrodynamics and mass transfer rates in a given system. However, the solution of PBE is not simple; in their general form, PBEs are complex integro-differential equations containing transient, convection, diffusion, and production/source terms.

The first step towards solving the PBE is reducing the terms encountered in the complete general form by making simplifying assumptions. Until today, no solution exists for the population balance equation in its most general form. Even for simplified PBEs, analytical solutions are rare and applicable only to very specific or further simplified situations. Furthermore, when an accurate representation of the real physical conditions is required, the birth and death rate functions, or source and sink terms, incorporated in the PBE can become highly complex. For this reason, most investigations rely on numerical and statistical methods of solution (Jairazbhoy and Tavlarides, 2000).

The birth and death rate kernels incorporated in the PBE are formulated based on the underlying theories and principles of breakage and coalescence. Liao and Lucas

(2010) listed the three theories behind bubble coalescence. The first is the film drainage model, where two bubbles must collide then remain in contact until the liquid film between them ruptures at a critical thickness. The second is the energetic collision model, where colliding bubbles immediately coalesce if the relative speed exceeds a critical value. The third is the critical approach velocity model, where small approach velocities lead to coalescence. According to the authors, the models for the coalescence frequency kernel can be divided amongst physical and empirical ones. The empirical models gave the coalescence frequency directly, while the physical ones gave it as a product of coalescence efficiency and collision frequency, which are in turn obtained based on the underlying theory of coalescence considered. It is worth noting, however, that the coalescence efficiency of the physical models based on the critical approach velocity theory was given as an empirical relation, while that based on the other theories was given by a physical relation. On the other hand, the collision frequency of the physical models was given as a physical relation for all three theories. The different expressions obtained resulted from the five different mechanisms promoting collision, namely turbulent random motion, velocity gradients, capture in turbulent eddies, buoyancy, and wake-entrainment. As for the breakage kernels, Liao and Lucas (2009) described the four mechanisms behind fluid particle breakup. These mechanisms can be summarized by breakup due to turbulent fluctuations and collisions, breakup due to viscous shear stress, shearing-off breakup, and breakup due to interfacial instability. Each mechanism or theory, or combination of mechanisms and theories, results in different breakage and coalescence representations. A literature review focused on the developments and applications of population balance modeling (PBM) for liquid-liquid and gas-liquid systems will be the main topic of the coming section.

2.2. Advances in PB Modeling

2.2.1. Advances in PB Modeling Applications

PB modeling has been used for several decades to understand and optimize certain industrial/engineering processes. With the start of the 21st century, PB applications began ranging from modeling the agglomeration and fragmentation of nano-particles (Sommer et al., 2006; Singh and Kumar, 2006) and colloidal fractals (Runkana and Kapur, 2006; Kim and Kramer, 2006) to the simulation of activated sludge flocculation (Ding et al., 2006). More recent applications can even extend to the modeling of crystal morphology, cell growth and differentiation, gene regulatory processes, and the transfer of drug resistance (Ramkrishna and Singh, 2014). The basis for these applications and others is the numerical solution of the partial integro-differential equation, along with the identification/optimization of any involved model parameters. With the increase in the number of solution methods to the PBE and in computer speed, as well as the advances in parallel computing, PB modeling has become increasingly widespread in various disciplines, especially in the chemical and process industries.

2.2.2. Advances in Methods of Solution

There exist several methods for the numerical solution of the population balance equation. The most commonly used ones are the quadrature-based methods of moments (QBMM), discretized PBE method (DPBE), fixed pivot method, cell average technique, finite element methods, the spectral solution method (including the Galerkin and

orthogonal collocation methods), and stochastic methods such as the Monte Carlo method.

The method of moments was first proposed by Hulburt and Katz (1964), based on writing the PBM in terms of the moments of the distribution of interest, but was not applicable until a solution to the closure problem was found by McGraw (1997). The latter applied the first method of moments, called the quadrature method of moments (QMOM) which progressed into an entire class of moment-based solutions labeled as quadrature-based moment methods (QBMM). To solve the PBE, the governing equations must be derived from the generalized PBE as a series of number, or probability, density functions. A probability density function (PDF) is defined at each node of the domain, or at each point of a given discretized particle property. Each of these nodes or points is multiplied by a weight, expressing the probability of having a particle at this node/point. These functions can then be easily coupled with existing, or altered, CFD solvers, by adding the necessary parameters to similar predefined functions. These solvers in turn provide a computationally efficient solution (Buffo et al., 2013).

The DPBE method began with the work of Batterham et al. (1981), and was elaborated by Hownslow and Marshall (1988). It began by discretizing the drop size domain into intervals with geometrically increasing sizes. Any daughter particle resulting from parent drop interactions was designated to one of these specific size classes based on its resultant size. If its actual size does not correspond exactly to one of the predetermined size classes, it is split by weights amongst the size classes just over and just under its actual size. The rate of change of the particle number is then written in terms of these number classes. The resulting equation is re-written in terms of particle

moments, leading to a discretized summation of ordinary differential equations. The latter can then be easily solved using various numerical techniques for differential equations (Hounslow et al., 1988).

The fixed pivot technique, originally developed by Kumar and Ramkrishna (1996a), involves discretizing the drop volume domain into a fixed number of elements which are termed "grid points", or "pivots". The overall particle population is then distributed over the fixed discrete points of the domain. Unlike the DPBE method, the pivots are not necessarily situated at geometrically increasing values. On the other hand, similarly to the DPBE method, if any resultant particle does not correspond to one of the grid points, the overall number of particles with this volume is distributed over the surrounding points in a way that preserves the overall volume. In each volume interval, the number density function is assumed constant, and is integrated to obtain the particle number distribution of the interval. The PBE is then expressed for each volume interval and integrated over each. The overall PBE describing the system is a summation of the resolved PBEs of each interval of the domain.

The cell average method was developed by Kumar et al. (2006) on the same basis as the fixed pivot method to solve the PBE. However, it resolved the fixed pivot technique's problem of overestimating the number density in the large size range in homogeneous systems. Instead of immediately assigning weights, or fractions, of the daughter bubble which does not conform to one of the pivots to its two neighboring pivots, the cell average method requires two steps: the average size of newborn bubbles in a specific interval is first calculated, and then they are assigned to adjacent pivots similarly to the former method.

Finite element methods can be traced back to the works of Hrennikoff (1941) and Courant (1943) and were eventually expanded to yield finite difference, finite element, and finite volume methods. These methods are based on discretizing the domain, either lengthwise (as in the case of the finite difference method), based on area (as in the finite element method), or based on volume (as in the finite volume method). To solve the PBE, each discrete element is considered separately. When fine elements are studied, approximations, such as assumptions of homogeneity, can be made with a higher degree of accuracy. These approximations allow the PBE to be easily solved in each domain element. The solution of the PBE over the entire domain is then obtained by summing the solutions of all the elements. Such solution methods were employed by numerous researchers, such as Mahoney and Ramkrishna (2002), Azizi and Al Taweel (2007), John et al. (2009) and others.

The spectral solution method was put forth in a series of papers by Steven Orszag in 1969. It can be used to solve partial differential equations, including the PBE. The solution is written as a summation of basis functions whose coefficients are repetitively changed until the differential equation is well satisfied. This method is numerically similar to the finite element method, but has a global approach and faster convergence when the solution is smooth. It includes individually used methods, such as the Galerkin, tau, orthogonal collocation, and least-square methods. Spectral solution methods were used by numerous researchers for various cases. Dorao and Jakobsen (2007) solved a spatially dependent PBE with advective terms using a high-order least-square method. Solsvik and Jakobsen (2016), on the other hand, solved a non-linear PBE with breakage and coalescence terms by implementing each of the orthogonal collocation, least-square, and Galerkin techniques.

The abovementioned orthogonal collocation method consists of transforming the partial differential PBE to a set of ordinary differential equations by using a truncated series expansion at a collocation point. The obtained set of equations can then be solved using the inbuilt solvers in existing software. The Galerkin method, also a finite element method, was put forth by Boris Galerkin in 1915. It is a numerical solution method which consists of finding an approximate solution for an operator equation. The operator equation may be a non-linear partial differential equation, which is the case of the PBE. The solution of the PBE is written as a linear combination of the elements of a linearly independent system with corresponding coefficients. These are resolved using sufficient boundary value conditions, and the coefficients are calculated by solving the resulting system of linear equations. This method was used in the works of Mantzaris et al. (2001) for the case of multi-variable population balance equations, and Ganesan (2011) for a high-dimensional PBE.

The dynamic evolution of the DSD in a particulate process can also be obtained by employing stochastic Monte Carlo (MC) simulations. Spielman and Levenspiel (1965) were the pioneers in using an MC approach to study particle coalescence in well-mixed two-phase reactors. Afterwards, Shah et al. (1977) formulated a general MC algorithm for time varying particulate processes. Then, Ramkrishna (1981) established the mathematical correlation between PBs and the MC approach. In MC simulations, a finite number of sampled particles is taken from the larger population, as opposed to studying the system altogether. The properties, or internal coordinates, of these sampled particles, randomly chosen, are simulated in a manner that involves the interactions between them. The properties of the larger population are then stochastically inferred from the sample.

Several reviews detailing the methods of solution of the PBE can be found in the literature (Ramkrishna, 1985; Dafniotis, 1996; Kumar and Ramkrishna, 1996a). Furthermore, other comparative studies of the various numerical solutions are also available (Kostoglou and Karabelas, 1994, 1995; Nicmanis and Hounslow, 1996; Alexopoulos et al., 2004; Alexopoulos and Kiparissides, 2005; Roussos et al., 2005; Meimaroglou et al., 2006). Based on these studies, the DPBE method of Litster et al. (1995), the fixed pivot method of Kumar and Ramkrishna (1996a), the Galerkin and the orthogonal collocation on finite-element methods were found to be the most accurate and stable techniques for the numerical solution of the PBE (Saliakas et al., 2008).

2.2.3. Kernel Development

A large number of breakage and coalescence models is available in the literature. These models are based on phenomenological, statistical, or empirical arguments. The review presented here is by no means extensive but rather focuses on the prominent works.

Coulaloglou and Tavlarides (1977) proposed a description for interaction processes in agitated liquid-liquid dispersions. They considered the flow to be isotropic at Reynolds numbers higher than 10,000, with the flow being subjected to a uniform, volume-averaged, energy dissipation rate. Their models were based on phenomenological observations, and they postulated that an oscillating deformed drop will break if the turbulent kinetic energy transmitted to it by a turbulent eddy, of comparable or smaller size, exceeds its surface energy. Additionally, they developed their coalescence model in analogy with the kinetic theory of gases. For coalescence to occur in a turbulent flow field, they considered that the drops must first collide then

remain in contact until the liquid film between them drains and ruptures. When compared with experimental data, they concluded that their model correlated satisfactorily with experiments, but that further testing was needed on various properties and operating conditions.

Luo and Svendsen (1996) put forth a novel model for fluid particle breakup in turbulent fluid-fluid dispersions, without resorting to the inclusion of adjustable parameters which, according to them, may affect the generality of the model. The authors begin by employing several simplifications. Firstly, they assume there to be an isotropic turbulence throughout the flow. Secondly, breakage is assumed to be binary only. Third, the breakage volume fraction is supposed to be a stochastic variable. Fourth, the possibility of breakup is attributed to the energy level of the arriving eddy. Finally, the authors assumed that only eddies of length scale less than or equal to the breaking particle can induce particle oscillations. They then wrote the general form of the breakage rate/frequency as the integral over the possible eddy lengths of the product of the collision frequency with the probability of breakup into two particles with specific sizes. Expressions for the latter two were then formulated. The collision frequency was based on the random motion of eddies, while the breakup probability was based on probability theory coupled with the initial assumptions. Finally, the daughter size distribution is expressed using the result of the former expression, based on the definition of a distribution. The formulated model was found to agree well with the experimental results of Hesketh et al. (1991) who studied a gas-liquid turbulent flow in a high-intensity pipeline. However, the authors recommend comparing the model to improved experimental studies for verification.

Martinez-Bazan et al. (1999) proposed a phenomenological breakup model based on the idea that the breakup frequency is proportional to the difference between the forces which cause bubble deformation on one hand, and those which cause confinement on the other hand. Although it was developed for the case of air in water dispersions, some investigators extended it to the case of liquid-liquid systems (Zaccone et al. 2007). Their proposed daughter distribution function follows an inverted U-shape curve with the highest probability for equal-sized breakage. Martinez-Bazan et al. (1999) found that their model predictions were in good agreement with experimental results for air bubbles injected in a turbulent water jet. Compared to various commonly used breakage kernels, Lasheras et al. (2002) found that this model provided the best agreement with experimental results. These findings were also validated by Martin-Valdepenas et al. (2007) when various models were compared in a CFD framework. However, Liao and Lucas (2009) noted that the validation of this model is still restricted to homogeneous and isotropic turbulent flows.

Lehr and Mewes (2001) presented new kernel functions for the rate of bubble breakup and coalescence which were then refined by Lehr et al. (2002). The binary breakup model which accounts for the daughter bubble size distribution was formulated based on the interaction between bubbles and turbulent eddies. The breakage density function uses only the capillary constraint (where the dynamic pressure of the turbulent eddy must be larger than the capillary pressure of the smaller daughter bubble formed) and assumes that the interfacial force on the bubble surface and the initial force of the colliding eddy balance each other. However, some investigators question this force balance, assuming that the inertial force of the colliding eddy during breakage is often larger than the interfacial forces of the bubble (Hagesaether et al., 2002; Wang et al.,

2003). The daughter distribution function predicts a maximum probability for equal-sized breakage when the mother drop/bubble is small relative to the maximum stable drop/bubble size. Contrastingly, unequal breakage is preferred as the size of the mother drop/bubble increases. Moreover, the coalescence model accounted for the characteristic velocities arising from both turbulent fluctuations (where the velocity is that of a turbulent eddy of the length scale of the bubbles) and the difference in rise velocities of bubbles of different size. However, collisions would only result in coalescence if the relative velocity of approach perpendicular to the surface of contact is lower than a critical velocity that must be determined empirically. The authors found the model capable of predicting the bubble size distribution (BSD) in bubble columns, with bimodal distributions being predicted for large superficial gas velocities. Furthermore, from the self-similarity of the calculated BSD, they reduced the PBE to balance equations for the average bubble volumes and volume fractions for both small and large bubbles, which can be used in conjunction with CFD.

Hagesaether et al. (2002a) introduced a particle breakup criterion based on the requirement that energy density cannot increase as a result of collision and breakup. This energy density criterion was found more important than the surface energy one in finding the breakup rate for large eddies colliding with fluid particles. In contrast, for small fluid particles, the surface energy criterion is important, while the breakup rate condition is severely limited. Moreover, the daughter size distribution follows directly from the model assumptions, such that it varies with fluid particle size, eddy size and energy level, and system variables. However, the spread of daughter particle sizes is larger for relatively large particles and large eddies than for small particles and small eddies. Hagesaether et al. (2002b) tested this model against bubble column experimental

results and found good agreement with the model predictions. However, no reasonable agreement between experimental data and BSD predictions was reached when the hydrodynamic and physico-chemical conditions inside the column were altered.

Similarly to Hagesaether et al. (2002a), Wang et al. (2003) assumed that the kinetic energy of the eddy colliding with the bubble must also be larger than the increase of the surface energy of the bubble during breakage. This was the only constraint considered in the model of Luo and Svendsen (1996), but it is in contrast with the force balance considered by Lehr et al. (2002). Furthermore, the theoretical breakup kernel proposed by Wang et al. (2003) is applicable to both gas-liquid and liquid-liquid systems, including a breakup distribution function that predicts the existence of a local minimum at exactly equal breakup with a dependence on the mother bubble/drop size and energy dissipation rates. Additionally, it goes to zero when the breakup fraction tends to zero and does not have a singularity point. This distribution function was also found to give good agreement with the experimental results reported by Hesketh et al. (1991) for gas-liquid flow in horizontal pipelines.

Razzaghi and Shahraki (2016) proposed a new generalized phenomenological breakage model based on the theories of probability and isotropic turbulence for multiple breakups in a turbulent flow field. This was done by modeling a succession of binary breakages to obtain a certain number of daughter drops, leading to a breakup probability function. The model made use of the energy density, as opposed to the energy as with former models, thus increasing the predicted breakage rate which was, according to the authors, underestimated in former models such as those of Luo and Svendsen (1996) and Zhao and Ge (2007). For the collision frequency, they used the specific collision frequency as opposed to the interaction frequency. Furthermore, for

the breakup probability, they added a restriction on the surface energy of the particle to the breakage criteria, such that the eddy energy density must be equal to or higher than the surface energy density of the smallest resulting daughter particle in order for breakage to occur. The model showed reasonable agreement with the experimental data of Zhang et al. (1992) for ternary breakup. The results also showed that ternary and quaternary breakups constitute over 90% of all fragmentation at low energy dissipation rates, while fragmentations of up to six daughter particles constitute over 95% of all fragmentation at higher energy dissipation rates.

Solsvik et al. (2017) formulated a novel breakage model by extending the breakage frequency model of Martinez-Bazan et al. (1999) to include the fact that only a fraction of the bubbles breaks at finite Reynolds numbers. They did so by incorporating the breakup probability suggested by Coualoglou and Tavlarides (1977) into their breakage frequency expression to give more physically realistic predictions of less intense turbulence systems. Simulations based on the obtained model were compared to the single bubble breakage experimental data of Solsvik and Jakobsen (2015c) obtained in a stirred tank operated with a Rushton turbine at stirring rates of 500, 600, and 700 rotations per minute corresponding to mean energy dissipation rates of the overall system of 0.5, 0.9, and 1.4 m^2s^{-3} respectively. They found that including the bubble breakage probability might have a significant effect on the model prediction of the bubble breakage frequency. However, they concluded that extensive experimental analyses are required to gather sufficient experimental data for improved understanding of the physical phenomena and for model validation. They specifically note that bubble breakage analysis must be performed simultaneously with the characterization of the local turbulence properties in the flow.

As previously stated, the aforementioned review is neither exhaustive nor complete. There exist some notable reviews in the literature that discuss the methods of solution of the PBE and the various available kernels in a much more detailed fashion.

For example, Lasheras et al. (2002) reviewed models for the breakage of an immiscible fluid immersed in a fully developed turbulent flow. The study focused on the case of no relative velocity between the phases, where fragmentation is only caused by turbulent velocity fluctuations. A comparative analysis of six commonly used breakup frequency models was presented along with a review of a large number of daughter distribution functions. These were classified based on the approaches used in determining them: statistical models, surface energy models based on eddy collisions, surface energy models based on stress balance, and hybrid models (combining both statistical and phenomenological models that are based on the surface energy of a breaking particle). However, while comparing the model predictions to the results of an experiment of an air in water turbulent jet (Martinez-Bazan et al., 1998, 1999a and b), only four models were selected. These findings were later validated by Martin-Valdepenas et al. (2007) where CFD, using a multi-fluid model that accounts for the relative velocity between the phases, was employed to repeat the earlier comparative study of Lasheras et al. (2002).

The advancements of the previous decade, along with the classical approaches used in the modeling of bubble column reactors, were broadly and extensively reviewed by Jakobsen et al. (2005). While emphasizing the population balance modeling of bubble coalescence and breakage processes, the progress in using averaged Eulerian multi-fluid models and CFD to model vertical bubble-driven flows was also presented. Furthermore, the authors discussed the limitations of the constitutive relations used to

describe the bubble-bubble and bubble-turbulence interactions, the bubble coalescence and breakage criteria, and the daughter size distribution models. They concluded that the limiting steps in model derivation are the proper formulations of boundary conditions, closure laws determining turbulence effects, interfacial transfer fluxes, and the bubble coalescence and breakage processes.

Liao and Lucas (2009) performed a thorough comparative review of most of the models available for drop and bubble breakup in turbulent dispersions. They described the mechanisms of fluid particle breakup, namely breakup due to turbulent fluctuation and collision, viscous shear stress, shearing-off, and due to interfacial instability. Then, they highlighted the various models for breakup frequency, and daughter-particle size distribution, which they classified according to their breakup criteria. These were then numerically compared against each other. For breakup frequency models, they noted that the predictions of the various models can differ by several orders of magnitude. For the DSD, they classified the models based on whether they are empirical, statistical, or phenomenological. Their conclusion was that the phenomenological models are the most reasonable, and that the M-shaped model used by Lehr et al. (1999, 2002), Wang et al. (2003) and Zhao and Ge (2007) gave the most reasonable results.

Liao and Lucas (2010) expanded their previous work to coalescence models. They classified these models based on their underlying theories, namely film drainage, energy collision, and critical approach velocity. The authors concluded that none of the existing coalescence models is capable of predicting the real situation, in addition to the fact that all model parameters are experiment specific. Subsequently, they recommended that the models be inclusive of all observed physical mechanisms and that the model parameters are generalized to a wider range of flows.

Solsvik and Jakobsen (2013) published a lengthy review on the constitutive equations of fluid particle breakup in multi-phase laminar and turbulent flows. They listed the four breakup mechanisms similarly to Liao and Lucas (2009), in addition to six criteria for breakup. They then reviewed the parameterizations for fluid particle breakup frequency based on each of the six criteria, and combinations of different criteria. The statistical and phenomenological models of particle size redistribution were then reviewed, followed by a survey for the experimental investigations pertaining to fluid particle breakup. This survey was followed by an investigation of breakage frequency and DSD models from the computational and applied points of view. They concluded that the development of the existing models is limited by the closure laws determining turbulence properties, interfacial transfer characteristics, and fluid particle coalescence and breakage processes. Also, the experimental investigations examined in their study indicate that multiple breakages are of utmost importance for droplet dispersions, and that the number of daughters created in a breakage event is also a topic that requires further elucidation. Furthermore, they found that all models were validated under particular circumstances, and that their generality is limited.

Deju et al. (2015) published a comparative analysis of coalescence and breakage kernels in vertical gas-liquid flow. They numerically assessed the six widely used kernels of Coulaloglou and Tavlarides (1977), Prince and Blanch (1990), Lehr et al. (2002), Luo and Svendsen (1996), Wang et al. (2003), and Martinez-Bazan et al. (1999a, 1999b). The predictions of different combinations of kernels taken from these models, found using the commercial CFD code ANSYS CFX12.1, were compared with the experimental values obtained from the gas-liquid vertical pipe TOPFLOW experiment of Lucas et al. (2010). Their results showed that the breakage kernels have

the greatest influence on the bubble size distribution, and that the effect of changing the coalescence kernels is minor. As their experimental data was limited, they were not able to clearly identify the most appropriate breakage and coalescence kernels. However, they expressed that most coalescence models predicted frequencies that are of the same order of magnitude near the wall region of the pipe, whereas the coalescence kernel of Coualoglou and Tavlarides (1977) gave slightly better predictions in the void fraction profile. On the other hand, they concluded that breakage kernels had more profound effects, which were attributed to the inherent nature of their breakage-dominated experiments. However, they concluded that the bell-shaped daughter size distribution, which favors equal-size breakage, over-predicts the BSD. In addition, they found that Luo and Svendsen's (1996) U-shaped DSD, which gives a maximum probability for low breakage fractions, to be unreasonable. The M-shaped daughter size distribution of Wang et al. (2003) was found to be the most physically acceptable distribution.

Furthermore, while testing the applicability of PBEs to various industrial processes, many investigators have resorted to the comparison of several models in the same work. Investigations dealing with the simulation of bubble columns, stirred tanks, rotating disk contactors, and pipe flows can be found numerous in the literature and have served as a showcase for the advancement of population balance modeling with or without CFD. A brief summary of some works that use PBEs for gas-liquid and liquid-liquid systems is presented here.

2.3. Gas-Liquid PB Applications

Petitti et al. (2010) modeled the BSD in a 194-L baffled gas-liquid stirred reactor, with two different types of spargers, using the PBE. The latter was solved using

the QMOM augmented by a novel correction algorithm, after coupling the PB model with CFD solvers. The flow field was described using an Eulerian-Eulerian approach with simplifications such as uniform bubble terminal velocity and drag force dependence on Sauter mean diameter instead of on the entire BSD. They employed the breakage and coalescence frequencies and the DSD put forth by Laakkonen et al. (2006), and the modified breakage kernel of Narsimhan et al. (1979). Finding that the spatial discretization of the transport equations leads to unphysical results, such as negative moments, the authors proposed a correction algorithm based on checking the convexity of the moments, then correcting them by replacing the corrupted moment sequence. Finally, they tested their method, after employing the moving reference frame approach, against a wide range of operating conditions with varying sparger design, stirrer speed, gas flow rate, and global holdup ranging from 0.2 to 7%. The predictions for the local gas holdup and distribution, as well as the BSD, were found to be accurate.

Buffo et al. (2013b) introduced a bivariate PB model into a CFD model, solved using the CFD code OpenFOAM, to simulate bubbly gas-liquid flow in a rectangular column. Their aim was to study the evolution of bubbles in real-space, time, and phase space (i.e. bubble size and composition). Even though the formulated problem was therefore complex, it was solved computationally efficiently by employing the conditional quadrature method of moments (CQMOM) where the number density function is assumed to be a summation of delta functions. They chose the breakage kernel of Alopaus et al. (2006) and Laakkonen et al. (2006, 2007) after refining the constants of their model. In parallel, they used the daughter distribution function proposed by Buffo et al. (2013a), which was a binary β -probability density function to account for the number of bubbles generated by breakage. On the other hand, they used

the coalescence kernels proposed by Coulaloglou and Tavlarides (1977) also after refining the model constants. For the mass transfer coefficient plugged into the CQMOM, the expression proposed by Lamont and Scott (1970) was used. The results were validated through a comparison with the experimental values obtained by Diaz et al. (2008a, 2008b), Cachaza Gianzo (2011), and Pflieger et al. (1999) and were considered sufficiently accurate to conclude that the coupling of QBMM with CFD seems promising for the simulation of poly-disperse multiphase systems in Eulerian frameworks.

At the start of 2018, Zhan et al. published a work on the effects of cell design and operating parameters on gas-liquid two-phase flows and bubble distribution characteristics in aluminum electrolysis cells, using a 3D CFD-PBM coupled model. The CFD solver was used to model the fluid flow, while the PBE was solved to find the DSD. They were then combined to find the Sauter mean diameter. For the PBE formulation, the kernels of breakage and coalescence used were those put forth by Luo and Svendsen (1996). The remaining parameters used were the drag force as in the Grace correlation, the turbulent dispersion force as in the Somonin correlation, the dispersed standard $k-\varepsilon$ (kinetic energy-energy dissipation) model, and a bubble-induced turbulence (BIT) model of Sato's eddy viscosity. The remaining parameters and operating conditions were based on the experimental setup used. They found that the increase of the anode-cathode distance results in a decrease in the bubble diameters. Also, they found that the bubble size increases with increasing anode width in almost all regions. However, with increasing anode length, it only increases in a small fraction of the central regions. On the other hand, the current density was found to have no effect

on the BSD. Finally, the authors found that the bubble size becomes smaller as the electrolyte depth increases, especially at the edge of the anode regions.

2.4. Liquid-Liquid PB Applications

In 2010, with the increase of reactor height vs. diameter especially in the PVC industry, Maaß et al. studied the drop sizes of liquid-liquid dispersions in slim reactors using empirical relations and the PBE, the latter being based on the compartment model approach for the energy distribution. For both approaches, the influence of physical parameters such as liquid level, stirrer speed and baffle length on the drop size and power consumption were studied. The empirical relations use the energy law for average energy dissipation, while the PBEs use two compartments, one around the impeller and one farther away, to give a more precise, non-homogeneous DSD. CFD simulations using the STAR-CCM+® software were used to determine the exact sizes of the two regions, and the unknown physical parameters involved. For the kernels of the PBE, they employed the model of Coualoglou and Tavlarides (1977). They then solved the PBE using the commercial solver PARSIVAL®. The empirical relations were found to only roughly predict the Sauter mean diameter. Similarly, the PBE using one homogeneous compartment gave only slightly better predictions. Contrastingly, the two-zone PBE approach yielded very satisfying results, with deviations less than 10% between the calculated and predicted Sauter mean diameters.

Amokrane et al. (2014) used CFD-PBE coupling to study drop behavior in a disc-donut pulsed column used for liquid-liquid extraction processes, which they extended to achieve continuous precipitation in a water-in-oil emulsion. They determined the appropriate turbulence model for the continuous phase in the pulsed

column using CFD simulations validated by particle image velocimetry (PIV). The most precise and computationally efficient turbulence model was found to be the standard k - ε model. On the other hand, the best kernels for breakage and coalescence used in the PBE were selected by performing homogeneous-type experiments in a stirred reactor. Those of Coualoglou and Tavlarides (1977), Martinez-Bazan et al. (1999) and Alopaeus et al. (2002) were found suitable and were used individually in formulating three separate PBEs. The parameters of these kernels were adjusted by fitting with the DSD measured in the stirred tank. The experimental values of the breakage parameters were lower, exhibiting the lower breakage tendency of their system. The resulting CFD-PBE model was implemented using QMOM in the CFD code ANSYS-Fluent® to determine the mean droplet size inside the column. The results were found encouragingly close to the experimental values, setting a good basis for future study, but Amokrane et al. concluded that they need further validation.

In 2017, Alzyod et al. (2017) published a paper on their steady state modeling of a Kühni liquid extraction column using the spatially mixed sectional quadrature method of moments (SM-SQMOM) in a one-dimensional domain. This method extended the SQMOM to solve the spatially distributed bivariate PBE in droplet diameter and solute concentration at steady state in order to study the hydrodynamics and mass transfer behavior of the Kühni column. The authors employed the coalescence kernels of Coualoglou and Tavlarides (1977) in their PBE. They developed an algorithm for their novel method, in which the resulting integral spatial numerical flux vector was closed using the Multi Primary one Secondary Particle Method, while the hydrodynamics integral source terms were closed using the analytical Two-Equal Weight Quadrature formula. On the other hand, to facilitate the source term implementation, an analytical

solution based on the algebraic velocity model was derived to calculate the required dispersed phase mean droplet velocity. Additionally, the authors coupled the hydrodynamic moment transport equations with the One Primary One Secondary Particle Method to close the mass transport equations. They finally solved the resulting system of ordinary differential equations using a fifth order numerical scheme in space. Their model predictions were validated against published experimental data for the DN80 Kühni extraction column. Alzyod et al. concluded that, using SQMOM, fifteen sections of the droplet diameter internal coordinate are enough to predict the droplet volume distribution and the column hydrodynamics in a way that matches the experimental data well. Furthermore, one section of the droplet solute concentration coordinate along the DSD was found enough to predict the mass transfer profiles along the Kühni column height.

CHAPTER 3

MATHEMATICAL MODELING

3.1. Population Balance Equation

Population balance equations describe the temporal variation in dispersed phase characteristics (e.g. size, mass, temperature, age, and species concentration) where the dispersed phase is considered as an assembly of drops/bubbles whose individual identities are continually destroyed and recreated by the dynamic processes occurring within the system. The extent of drop/bubble breakage and coalescence in turbulently flowing liquid–liquid, or gas–liquid, mixtures thus governs the evolution of the drop/bubble size distribution in the dispersion, and consequently the interfacial area of contact between the phases. In such systems, the hydrodynamics and the interfacial forces are the major factors affecting the changes in the interfacial area of contact between the phases. Consequently, breakage and coalescence processes take place simultaneously until a quasi-equilibrium state is reached, where the dispersion and coalescence rates become comparable and no net changes in drop/ bubble size and drop/bubble size distribution are observed. The use of population balance modeling (PBM) on these processes leads to an integro-partial-differential equation for which there exist very limited analytical solutions. When available, these analytical solutions are usually obtained at the expense of assuming unrealistic major simplifications (Azizi and Al Taweel, 2010).

In this work, assuming there is no convection in and out of the control volume, the discretized PBE will be used as presented by Coualoglou and Tavlarides (1977),

$$\begin{aligned}
\frac{\partial [N(t)A(d_j, t)]}{\partial t} &= B_b(d_j, t) - D_b(d_j, t) + B_c(d_j, t) - D_c(d_j, t) \tag{1} \\
&= N(t) \int_{d_j}^{d_{\max}} \beta(d_i, d_j) v(d_i) g(d_i) A(d_i, t) dd_i - N(t) g(d_j) A(d_j, t) \\
&\quad + [N(t)]^2 \int_0^{d_j/2^{1/3}} h_c \left((d_j^3 - d_i^3)^{1/3}, d_i \right) \\
&\quad \times \lambda_c \left((d_j^3 - d_i^3)^{1/3}, d_i \right) A \left((d_j^3 - d_i^3)^{1/3}, t \right) A(d_i) d_j^2 dd_i \\
&\quad - [N(t)]^2 A(d_j, t) \int_0^{(d_{\max}^3 - d_j^3)^{1/3}} h_c(d_j, d_i) \lambda_c(d_j, d_i) A(d_i, t) dd_i
\end{aligned}$$

Where, $N(t)$ is the total number of bubbles in the system, and $A(d_j, t)$ is the probability density of a bubble of diameter d_j at a time t . The product of $N(t)$ and $A(d_j, t)$ derived with respect to time gives the time variation of the total number of bubbles of diameter d_j at a time t . B_b , D_b , B_c , and D_c are the birth rate by breakage, death rate by breakage, birth rate by coalescence, and death rate by coalescence, respectively. The first two terms on the right hand side respectively represent the rate of formation and loss of drops/bubbles of diameter d_i due to breakage, where, $g(d_i)$ is the breakage frequency, $v(d_i)$ is the number of dispersed fluid entities formed from the breakage of bubbles of size d_i , and $\beta(d_i, d_j)$ is the size distribution of daughter drops/bubbles formed from the breakage of a drop/bubble of size d_i . The following two terms represent the rate of formation and loss of drops/bubbles of size d_i due to coalescence, respectively. Here, $\lambda_c(d_j, d_i)$ is the coalescence efficiency between drops/bubbles of sizes d_j and d_i , and $h_c(d_j, d_i)$ is the collision frequency between those of sizes d_j and d_i (Azizi and Al Taweel, 2010).

This work incorporates the coalescence and breakage kernels used by Wang et al. (2005a) into the PBE algorithm proposed by Azizi and Al Taweel (2010) to solve Equation (1), taking into consideration coalescence and breakage due to turbulent eddies only. In the sections below, the kernels of Coulaloglou and Tavlarides (1977) and Wang et al. (2003, 2005a) will be elaborated and compared.

3.2. The Kernels of Coulaloglou and Tavlarides (1977)

3.2.1. Coalescence Terms

The coalescence rate is defined as the product of a coalescence frequency, h_c , and a collision efficiency, λ_c , each of which has a multitude of models that describe it (Liao and Lucas, 2010).

3.2.1.1. Collision Frequency

By analogy with the collision of molecules as described by the kinetic theory of gases, the collision frequency was expressed as:

$$h_c(d_i, d_j) = C_3(d_i + d_j)^2(d_i^{2/3} + d_j^{2/3})^{1/2} \frac{\varepsilon^{1/3}}{(1 + \Phi_d)} \quad (2)$$

where C_3 is an empirical model parameter having different optimum values depending on the system. d_i and d_j are the diameters of the two coalescing bubbles/drops.

In the above expression, $(d_i + d_j)^2$ represents the collision-sectional area of the colliding bubbles, with the $\frac{\pi}{4}$ for area included in the constant. The larger the area is, the more frequent the collisions are. The second factor, $(d_i^{2/3} + d_j^{2/3})^{1/2}$, comes from the

mean-square root of the colliding bubble velocities, where the velocities are taken to be proportional to $v^{2/9}$, i.e., $d^{2/3}$ where v is volume and d is diameter. Similarly, the higher the speed of collision is, the more frequently collisions will occur. ε , which comes from the abovementioned velocity, with the power 1/3 dependence, is the energy dissipation. It represents the intensity of the turbulence in the continuous phase. The higher the energy dissipation, the higher the turbulence, and hence the higher the prevalence of turbulent eddies in the continuous phase. Accordingly, the frequency of bubble collisions increases, as well as the bubble-eddy collision frequency.

The term $(1 + \Phi_d)$ accounts for the fact that the dispersed phase dampens the intensity of turbulence in the continuous phase, with increased dampening as the volume fraction of the dispersed phase, Φ_d , increases. This was a correction incorporated by Hsia and Tavlarides (1980) and was not in the initial work of Coualoglou and Tavlarides (1977).

3.2.1.2. Coalescence Efficiency

Coualoglou and Tavlarides (1977) express this quantity as follows:

$$\lambda_c(d_i, d_j) = \exp \left[-C_4 \frac{\mu_c \rho_c \varepsilon}{\sigma^2 (1 + \Phi_d)^3} \left(\frac{d_i d_j}{d_i + d_j} \right)^4 \right] \quad (3)$$

where C_4 is another empirical model parameter having different optimum values depending on the system, and $(1 + \Phi_d)^3$ is a geometric correction, representing turbulence dampening, added later on. μ_c is the viscosity of the continuous phase. The above is a decaying exponential function of the ratio of the contact time and the

coalescence time. Coualoglou and Tavlarides refer to the expressions of Levich (1962) for the former, and Chappellear (1963) for the latter.

3.2.2. Breakage Terms

Coualoglou and Tavlarides (1977) assumed that breakage occurs on a certain premise. That is, an oscillating deformed drop will break only if the turbulent kinetic energy transmitted to it by turbulent eddies exceeds the drop's surface energy.

3.2.2.1. Breakage Rate

Coualoglou and Tavlarides give an expression for the breakage rate directly, without previous decomposition into collision frequency and breakage probability. Also, they name this term "the breakage frequency" as opposed to "the breakage rate" in their publications. They express this quantity as:

$$g(d) = C_1 \frac{\varepsilon^{1/3}}{d^{2/3}(1 + \Phi_d)} \exp \left[-C_2 \frac{\sigma(1 + \Phi_d)^2}{\rho_d \varepsilon^{2/3} d^{5/3}} \right] \quad (4)$$

where C_1 and C_2 are the breakage model parameters which also differ in optimal values depending on the system under study. Similarly to the coalescence kernels, the breakage rate also has the $(1 + \Phi_d)$ geometric correction for turbulence dampening. This model predicts a maximum breakage rate as the drop size increases. However, for gas-liquid mixtures, it predicts a breakup frequency that is several orders of magnitude lower than experimental results.

3.2.2.2. Daughter Size-Distribution

Coulaloglou and Tavlarides denote this kernel by “breakage distribution function”. It does not depend on the other breakage kernels, and can therefore be obtained directly from the diameters, before the previous calculation of the breakage frequency and efficiency/probability. However, this expression is a statistical model based on the assumption of a normal density function, less reasonable than the phenomenological models (Liao and Lucas, 2009). It goes according to:

$$\beta(d_i, d_j) = \frac{4.6}{d_j^3} \times \exp \left[-4.5 \frac{(2d_i^3 - d_j^3)^2}{(d_j^3)^2} \right] \quad (5)$$

Hsia and Tavlarides (1980) proposed a correction to the former daughter size-distribution, used in the algorithm of Azizi and Al Taweel (2010):

$$\beta(d_i, d_j) = 90 \frac{d_i^2}{d_j^3} \left(\frac{d_i^3}{d_j^3} \right)^2 \left(1 - \frac{d_i^3}{d_j^3} \right)^2 \quad (6)$$

This expression is able to completely account for the total volume of the fragments within the upper and lower diameter bounds (Azizi and Al Taweel, 2010). It is a beta distribution which produces a zero probability for infinitely small daughter drops and the daughter drops with equal size to that of the mother drop (Azizi and Al Taweel, 2011).

3.3. The Kernels of Wang et al. (2003, 2005a)

3.3.1. Coalescence Terms

Similarly to Coualaloglou and Tavlarides (1977), the coalescence rate is expressed as the product of collision frequency, h_c , and the collision probability/efficiency, λ_c .

3.3.1.1. Collision Frequency

Wang et al. (2005a) built on the model for collision frequency proposed by Prince and Blanch (1990) who developed it by analogy to the kinetic gas theory. The original model described the coalescence frequency as,

$$h_c(d_i, d_j) = \frac{\pi}{4} (d_i + d_j)^2 (\bar{u}_i^2 + \bar{u}_j^2)^{1/2} \quad (7)$$

where \bar{u}_i and \bar{u}_j are the mean speeds of the two coalescing bubbles/drops of diameters d_i and d_j respectively.

In the above expression, $\frac{\pi}{4} (d_i + d_j)^2$ represents the collision-sectional area of the colliding bubbles. The second factor, $(\bar{u}_i^2 + \bar{u}_j^2)^{1/2}$, represents the mean-square root of the colliding bubble velocities. Because bubble turbulence is mainly due to turbulent eddies, the mean turbulent velocity of a bubble of size d_i was assumed equal to the mean turbulent velocity of an eddy of the same size. According to Levich (1962), this velocity can be written as,

$$\bar{u}_i = \sqrt{2}(\varepsilon d_i)^{1/3} \quad (8)$$

Equation (8) describes the mean turbulent eddy velocity as obtained by applying classical turbulent theories (Liao and Lucas, 2010), where ε is the rate of turbulent energy dissipation.

Wang et al. (2005a) refined the above expression for collision frequency, Equation (7), by including two effects, namely the effect of the reduction of the free space for bubble movement due to the volume occupied by the bubbles themselves, and the effect of the ratio of the distance between bubbles and the bubble turbulent path length:

$$h_c(d_i, d_j) = \frac{\pi}{4} \frac{\Phi_{d,\max}}{\Phi_{d,\max} - \Phi_d} \Gamma_{ij} \sqrt{2} (\varepsilon d_i)^{1/3} (d_i + d_j)^2 (d_i^{2/3} + d_j^{2/3})^{1/2} \quad (9)$$

The reduction of free space for bubble/drop movement results in an increase in collision frequency. This is described by the factor $\frac{\Phi_{d,\max}}{\Phi_{d,\max} - \Phi_d}$, in place of the dampening factor of Hsia and Tavlarides (1980) mentioned above, where Φ_d is the dispersed gas holdup, and $\Phi_{d,\max}$ is its maximum possible value, which is the limit of close packed bubbles. Accordingly, it was determined as 0.8 in the work of Wang et al. (2005a). On the other hand, when the distance between bubbles/drops exceeds the bubble turbulent path length, the collision frequency is less than that obtained using Equation (7). To account for this, the empirical correlation denoted by Γ_{ij} was introduced into the equation. It depends on the ratio of the distance between bubbles and the bubble turbulent path length, such that Γ_{ij} approaches unity when the ratio is small and zero when it is large:

$$\Gamma_{ij} = \exp(-(h_{b,ij}/l_{bt,ij})^6) \quad (10)$$

$h_{b,ij}$ is the distance between the bubbles, related to the mean distance between the bubbles of size d_i and d_j by:

$$h_{b,ij} = k(n_i + n_j)^{-1/3} \quad (11)$$

where:

$$n_i = N_i/\Delta d_i \quad (12)$$

and N_i and Δd_i are the bubble number and the diameter increment in the i th bubble size region respectively, with the proportionality factor k set to 6.3 based on the measured bubble size distribution considered by Wang et al. (2005a). $l_{bt,ij}$ is the mean relative turbulent path length of bubbles of sizes d_i and d_j , such that:

$$l_{bt,ij} = (l_{bt,i}^2 + l_{bt,j}^2)^{1/2} \quad (13)$$

Each individual turbulent path length is assumed to be equal to the distance that a turbulent eddy of size λ and mean speed \bar{u}_{bt} moves during its lifetime τ_e :

$$l_{bt} = \bar{u}_{bt}\tau_e \approx 0.89\lambda \quad (14)$$

3.3.1.2. Coalescence Efficiency

Wang et al. (2005a) used the model formulated by Chesters (1991) which states that two colliding bubbles will coalesce only if the contact time (τ_{ij}) exceeds the coalescence time required for the liquid film between them to rupture (t_{ij}). Thus the coalescence efficiency/ probability is expressed as:

$$\lambda_c(d_i, d_j) = \exp\left(-\frac{t_{ij}}{\tau_{ij}}\right) \quad (15)$$

which is a decaying exponential function as with Coulaloglou and Tavlarides. To express τ_{ij} and t_{ij} , the authors employed the expressions proposed by Luo and Svendsen (1996b), which are based on an energy conservation analysis, resulting in:

$$\lambda_c(d_i, d_j) = \exp\left(-\psi \frac{(0.75(1 + \xi_{ij}^2)(1 + \xi_{ij}^3))^{1/2}}{(\rho_d/\rho_c + \gamma)(1 + \xi_{ij})^3} We_{ij}^{1/2}\right) \quad (16)$$

where ξ_{ij} is the ratio of bubble/drop diameters:

$$\xi_{ij} = d_i/d_j \quad (17)$$

We_{ij} is the Weber number defined as:

$$We_{ij} = \rho_c d_i \bar{u}_{ij}^2 / \sigma \quad (18)$$

In the above expressions, ρ_c and ρ_d are the densities of the continuous and dispersed phases, respectively, σ is the surface tension, and \bar{u}_{ij} is the mean-square root of the colliding bubble velocities expressed as:

$$\bar{u}_{ij} = (\bar{u}_i^2 + \bar{u}_j^2)^{1/2} \quad (19)$$

The virtual mass coefficient γ was set to 0.5 as with Maxey and Riley (1983) to account for the additional force which the accelerating and decelerating particles contribute to their surroundings, and the model parameter ψ , of order unity, was set to 1.0 because the influence of its variation amongst the proposed values is minimal (Wang et al., 2005b), and the value of 1.0 is the simplest in these calculations.

The resulting expression of Wang et al. predicts smaller coalescence efficiencies for smaller bubbles. In addition, it shows a much less steep decreasing trend than that of Coualoglou and Tavlarides.

3.3.2. Breakage Terms

In their model for breakage due to eddy collisions, Wang et al. (2003) took into account both the energy and the capillary force constraints to study the eddy-bubble interaction mechanism, instead of one fixed premise as did Coualaloglou and Tavlarides.

3.3.2.1. Breakage Rate

The specific bubble breakage rate was based on the work of Luo and Svendsen (1996b) whose model is based on the theories of isotropic turbulence and probability:

$$g(d) = \int_0^{0.5} b(f_v|d)df_v \quad (20)$$

where $b(f_v|d)$ is the breakage rate of a bubble of diameter d breaking with breakup fraction, or ratio of daughter drop to mother drop, f_v (which is taken to be from 0 to 0.5 instead of 1 due to the symmetry at 0.5) expressed as:

$$b(f_v|d) = 0.923(1 - \Phi_d)\varepsilon^{1/3} \times \int_{\lambda_{\min}}^d P_b(f_v|d, \lambda) \frac{(\lambda + d)^2}{\lambda^{11/3}} d\lambda \quad (21)$$

The lower bound of the integral, λ_{\min} is the minimum eddy size effective for bubble breakup. As opposed to Coualaloglou and Tavlarides, Wang et al. do not give an expression for the breakage rate directly. They first decompose this term into collision frequency and breakage probability, resulting in a more accurate expression yielding closer values to experimental results. The above expression is the product of collision frequency of bubbles with eddies and the breakage probability, elaborated below.

3.3.2.1.1. Bubble-Eddy Collision Frequency

In their work, Wang et al. (2003) used an expression for the collision frequency between the dispersed phase bubbles and the eddies in the continuous phase that is similar to the one they used for coalescence. It is also built on the analogy with the kinetic theory of gases.

$$h_c = \frac{\pi}{4} (d + \lambda)^2 \bar{u}_\lambda n_\lambda \quad (22)$$

Where, similarly to the coalescence case, $\frac{\pi}{4} (d + \lambda)^2$ accounts for the common surface area between the particles, d and λ are the drop and eddy diameters respectively, \bar{u}_λ is the mean kinetic energy of eddies of size λ , found using Equation (8), and n_λ is the number density of eddies of size λ expressed as:

$$n_\lambda = \frac{0.822(1 - \Phi_d)}{\lambda^4} \quad (23)$$

In the latter expression, Φ_d is the dispersed phase volume fraction. The factor $(1 - \Phi_d)$ is introduced because turbulent eddies only exist throughout the continuous phase (Xing et al., 2014). λ^4 gives the volume at the eddy scale, per particular eddy diameter, and the 0.822 in the expression is a constant concluded from observations. Thus, the collision frequency between a bubble/drop of diameter d and a turbulent eddy of diameter λ becomes,

$$h_c = 0.923(1 - \Phi_d)\varepsilon^{1/3} \frac{(\lambda + d)^2}{\lambda^{11/3}} \quad (24)$$

3.3.2.1.2. Breakage Probability Density

$P_b(f_v|d, \lambda)$ is the breakup probability density for a bubble of size d to break into a fraction f_v when hit by an eddy of size λ . This is expressed as,

$$P_b(f_v|d, \lambda) = \int_{e(\lambda)_{\min}}^{e(\lambda)_{\text{cutoff}}} P_b(f_v|d, e(\lambda), \lambda) P_e(e(\lambda)) de(\lambda) \quad (25)$$

where $e(\lambda)$ is the eddy energy which can vary from $e(\lambda)_{\min}$ to $e(\lambda)_{\text{cutoff}}$. The authors assumed that the probability of having an eddy with kinetic energy greater than $10\bar{e}(\lambda)$ is negligible (Wang et al., 2004). Therefore, the cutoff value was set to,

$$e(\lambda)_{\text{cutoff}} = 10\bar{e}(\lambda) \quad (26)$$

where $\bar{e}(\lambda)$ is the mean kinetic energy of the eddies, expressed as:

$$\bar{e}(\lambda) = \frac{\pi}{6} \lambda^3 \rho_c \frac{\bar{u}_\lambda^2}{2} \quad (27)$$

In turn, $e(\lambda)_{\min}$ depends on the region of the flow. As f_v ranges between 0 and 0.5, the flow passes from the surface energy controlled region (where breakage is dictated by surface energy) to the capillary pressure controlled region (where breakage is dictated by capillary pressure). In the first region, $e(\lambda)_{\min}$ is found using:

$$e(\lambda)_{\min} = \left(f_{v,\min}^{2/3} + (1 - f_{v,\min})^{2/3} - 1 \right) \pi d^2 \sigma \quad (28)$$

where $f_{v,\min}$ is the minimum breakage fraction in the chosen sub-region, expressed in the surface energy controlled region as:

$$f_{v,\min} = \left(\frac{\pi \lambda^3 \sigma}{6e(\lambda)d} \right)^3 \quad (29)$$

and σ is the drop/bubble surface tension. In the second region, $e(\lambda)_{\min}$ is found using:

$$e(\lambda)_{\min} = \frac{\pi\lambda^3\sigma}{6f_{v,\min}^{1/3}d} \quad (30)$$

$f_{v,\min}$ in the capillary-pressure controlled region is found iteratively from zero through the sub-regions.

In Equation (25), the probability of a droplet of size d breaking with breakup fraction f_v is determined by:

$$P_b(f_v|d, e(\lambda), \lambda) = \begin{cases} \frac{1}{f_{v,\max} - f_{v,\min}} & \text{and } f_{v,\max} - f_{v,\min} \geq \delta, \\ 0 & \text{else} \end{cases} \quad (31)$$

where δ was taken to be 0.01 by Wang et al. (2003) to avoid sudden spiking in the solution. $f_{v,\min}$ is found according to the region as mentioned above, and $f_{v,\max}$ is found by solving the equation:

$$\left(f_{v,\max}^{2/3} + (1 - f_{v,\max})^{2/3} - 1\right) \pi d^2 \sigma = e(\lambda) \quad (32)$$

The term for the energy distribution of eddies of size λ in the breakup probability density expression, Equation (25), goes as follows:

$$P_e(e(\lambda)) = \frac{1}{\bar{e}(\lambda)} \exp(-e(\lambda)/\bar{e}(\lambda)) \quad (33)$$

This expression was derived by Angelidou et al. (1979) based on probabilistic arguments pertaining to the energy distribution of drops/bubbles in a continuous fluid. It decreases exponentially with an increase in $e(\lambda)$.

The resultant expression of the bubble/drop breakage rate is:

$$\begin{aligned}
g(d) = & \int_0^{0.5} 0.923(1 \\
& - \Phi_d)\varepsilon^{1/3} \\
& \times \int_{\lambda_{\min}}^d \int_{e(\lambda)_{\min}}^{e(\lambda)_{\text{cutoff}}} \frac{1}{f_{v,\max} - f_{v,\min}} \frac{1}{\bar{e}(\lambda)} \exp(-e(\lambda)) \\
& / \bar{e}(\lambda)) de(\lambda) \frac{(\lambda + d)^2}{\lambda^{11/3}} d\lambda df_v
\end{aligned} \tag{34}$$

for $f_{v,\max} - f_{v,\min} \geq \delta$ and $f_{v,\min} < f_v < f_{v,\max}$, and zero otherwise.

3.3.2.2. Daughter Size-Distribution

The daughter bubble size-distribution is expressed by Wang et al. (2003) according to the following expression:

$$\beta(f_v, d) = \frac{b(f_v, d)}{\int_0^{0.5} b(f_v, d) df_v}. \tag{35}$$

The above expression is a phenomenological M-shaped model formulated based on the underlying physical observations of the effect of the capillary pressure on the formation of small daughter droplets. It predicts a probability that tends to zero when the breakup fraction falls below a certain small value (Wang et al., 2003), similarly to Coualoglou and Tavlarides (1977). However, unlike the model of Coualoglou and Tavlarides, this kernel predicts a lower probability of equi-sized breakup.

CHAPTER 4

NUMERICAL SOLUTION AND RESULTS

4.1. Numerical Solution of PBE and Coefficient Optimization

After the compilation of the mathematical formulation required for the PBEs in this study, methods of solution were put together and implemented. In the first part of the work, the PBE was written as expressed by Coualoglou and Tavlarides (1977), with the omission of the convection terms, and the addition of the corrective adjustments made by Hsia and Tavlarides (1980). The coefficients of breakage and coalescence ($C_1 - C_4$) in the PB model were optimized under various hydrodynamic conditions as elaborated below. In the second part, the model of Wang et al. (2003), with the kernels elaborated by Wang et al. (2005a), was implemented. A numerical solution method was proposed based on the algorithms put forth by Wang et al. (2004) and the improvements made by Razzaghi and Shahraki (2011), in conjunction with the algorithm of Azizi and Al Taweel (2010).

4.1.1. Solution Methodology

4.1.1.1. Coefficient Optimization

To optimize the coefficients found in the abovementioned PBE model, the algorithm put forth and refined by Azizi and Al Taweel (2010), as shown in Figure 1, was implemented in MATLAB. All the information required for initializing the PBE solution (e.g. physical properties of the two phases, initial drop/bubble size distribution, hydrodynamic and interfacial parameters, computational parameters, and the flags

necessary to select appropriate/desired coalescence and breakage models) are first inputted into the program. Based on these initial conditions, the various breakage and coalescence rates, and the net rates of change of number density, are calculated for all sample points. Using suitable integration subroutines, the new DSD predicted to occur at $t + \delta t$ is calculated. This process is repeated until the maximum integration time is reached. Information concerning the DSD is periodically sampled in order to determine the temporal variation in DSD, the interfacial area of contact and the values of the various mean diameters (Azizi and Al Taweel, 2010).

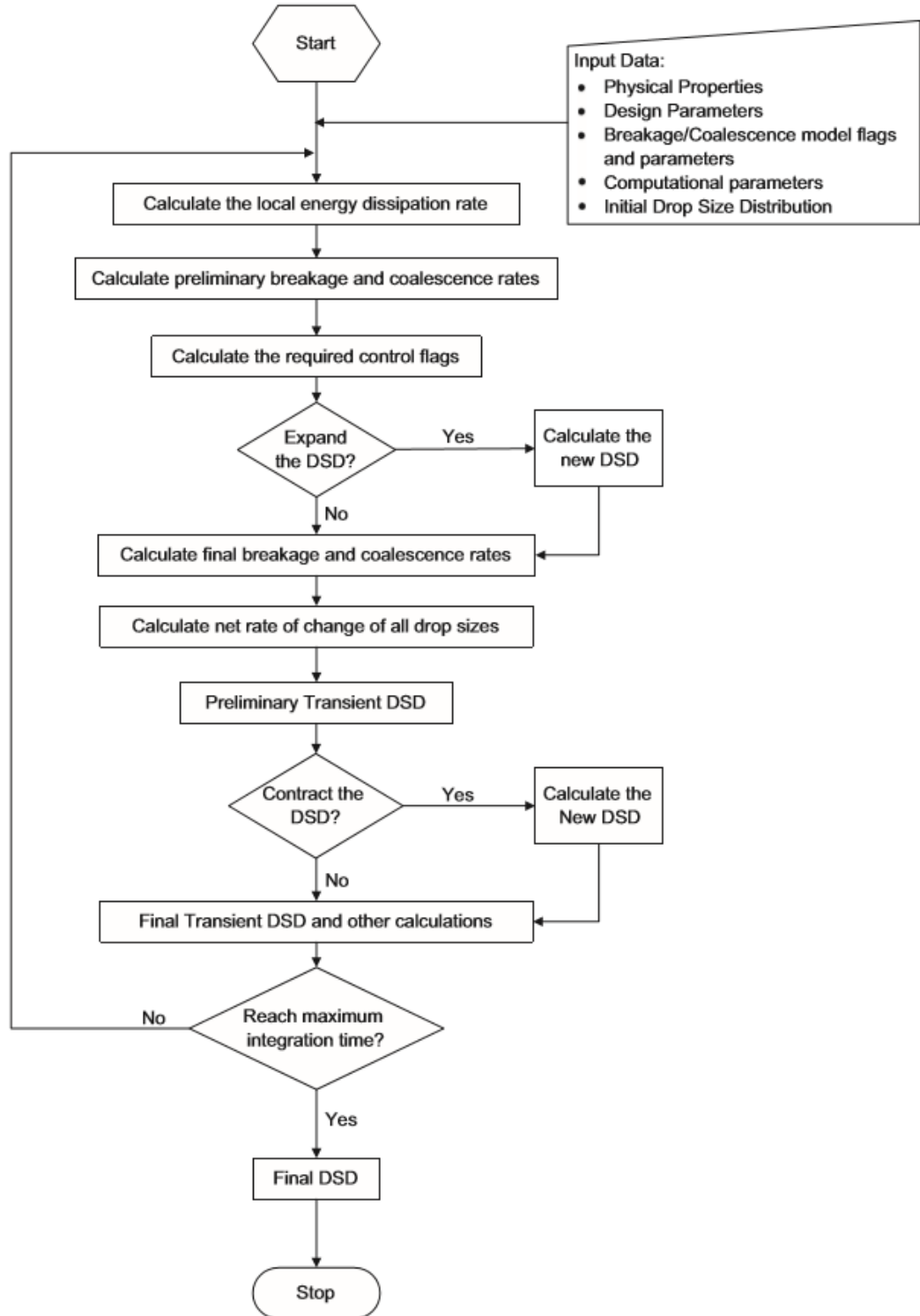


Figure 1: Overall Algorithm for Solving the PBE (Azizi and Al Taweel, 2010)

To run the code for optimization, a main was created with a function for finding the sum of least squares of a non-linear equation, as is the case of the PBE, using the Levenberg-Marquardt minimum-finding algorithm. The experimentally measured Sauter mean values obtained by Azizi and Al Taweel (2007), $d_{32,exp}$, were subtracted from the Sauter mean diameters obtained using the kernels of Coulaloglou and Tavlarides (1977), $d_{32,sim}$. The sum of the squares of these subtractions formed the objective function for the optimization:

$$\min_c \|F(K)\|_2^2 = \min_c \sum_i (d_{32,sim} - d_{32,exp})^2 \quad (36)$$

The optimization was run for various surfactant concentrations, at specified flow speeds and gas holdups. Each combination of concentration, speed, and holdup had its own set of experimental data. The resultant values of the optimized constants for the different variable combinations are tabulated in the result section below. These constants were then used as input to the PBE function for the same values of surfactant concentration for which they were obtained, but for different values of holdup and flow speed, to obtain simulated values of the resultant Sauter mean diameters for the different conditions. The latter were each graphed against the corresponding set of experimental values of the Sauter mean measured under the same flow conditions. These graphs are found in the result section of this chapter.

4.1.1.2. Solving for the Kernels of Wang et al. (2003, 2005a)

The physical models of breakage and coalescence put forth by Wang et al. (2003, 2005a) were integrated into the algorithm of Azizi and Al Taweel (2010) in order to study the applicability of the models to the experimental conditions studied by the

latter. To do so, the necessary parameters were added to the experimental input, and the mathematical formulations of the models were encoded as an addition to the initial MATLAB code used in the previous section. These were combined with the existing parts of the algorithm, with the addition of some necessary subroutines for the Wang et al. model specifically.

The coalescence kernels were determined through direct numerical integration following domain discretization and integral boundary determination. However, due to the time-consuming triple integral found in the breakage frequency term of their formulation, Equation (34), the efficient numerical algorithm to reduce the triple integral to a double integral proposed by Wang et al. (2004) was also incorporated into Azizi and Al Taweel's algorithm. Their proposition begins by considering the breakup fraction range, $f_v \in [0,0.5]$. They split this range into two sub-regions based on the dominant physical constraint in each of the latter. In the first region, in the smaller f_v range, the capillary pressure constraint is dominant, while in the second region, the surface energy constraint is dominant. The two regions meet where the f_v calculated using the capillary pressure constraint is equal to that calculated based on the surface energy constraint. This common value of f_v is denominated "critical breakup fraction", denoted by f_{vc} , and obtained by solving the following equation:

$$f_{vc}(f_{vc}^{2/3} + (1 - f_{vc})^{2/3} - 1)^3 = \frac{1}{6^3} \left(\frac{\lambda}{d}\right)^9. \quad (37)$$

After finding the domain of the capillary pressure controlled region, $f_v \in [0, f_{vc}]$, and that of the surface energy controlled region, $f_v \in [f_{vc}, 0.5]$, Wang et al. (2004) set out to find the breakage probability density $P_b(f_v|d, \lambda)$, Equation (20), in each of the two regions. In the first sub-region, the f_v domain is divided into finite

difference elements small enough to ensure precision, yet large enough to avoid unnecessary computation. The second sub-region is divided similarly. In this work, 30 elements were taken in each sub-region.

In the first sub-region, $P_b(f_v|d, \lambda)$ is calculated recursively forward from $f_{v,0} = 0$ to f_{vc} . The lower boundary is set to zero, such that $P_b(f_{v,0}|d, \lambda) = 0$. The first iteration is found by the following expression:

$$\begin{aligned}
 & P_b(f_{v,1}|d, \lambda) & (38) \\
 & = \begin{cases} \int_{e(\lambda)_1}^{e(\lambda)_{\text{cutoff}}} P_b(f_v|d, e(\lambda), \lambda) P_e(e(\lambda)) de(\lambda), & e(\lambda)_1 < e(\lambda)_{\text{cutoff}} \\ 0, & e(\lambda)_1 \geq e(\lambda)_{\text{cutoff}} \end{cases}
 \end{aligned}$$

The following iterations are found according to:

$$\begin{aligned}
 P_b(f_{v,i+1}|d, \lambda) &= \int_{e(\lambda)_{i+1}}^{e(\lambda)_{\text{cutoff}}} P_b(f_v|d, e(\lambda), \lambda) P_e(e(\lambda)) de(\lambda) & (39) \\
 &= \int_{e(\lambda)_{i+1}}^{e(\lambda)_i} P_b(f_v|d, e(\lambda), \lambda) P_e(e(\lambda)) de(\lambda) \\
 &+ \int_{e(\lambda)_i}^{e(\lambda)_{\text{cutoff}}} P_b(f_v|d, e(\lambda), \lambda) P_e(e(\lambda)) de(\lambda) \\
 &\approx (e(\lambda)_i - e(\lambda)_{i+1}) P_b\left(f_{v,i+\frac{1}{2}}|d, e(\lambda)_{i+\frac{1}{2}}, \lambda\right) \times P_e\left(e(\lambda)_{i+\frac{1}{2}}\right) \\
 &+ P_b(f_{v,i}|d, \lambda)
 \end{aligned}$$

In the above expression, $e(\lambda)_i$ is found according to:

$$e(\lambda)_i = \frac{\pi \lambda^3 \sigma}{6 f_{v,i}^{1/3} d} \quad (40)$$

and:

$$e(\lambda)_{i+1/2} = \frac{(e(\lambda)_i + e(\lambda)_{i+1})}{2} \quad (41)$$

As for the value of the breakup probability above, it is obtained according to:

$$P_b(f_{v,i+1/2}|d, e(\lambda)_{i+1/2}, \lambda) \quad (42)$$

$$= \begin{cases} \frac{1}{f_{v,i+1/2,\max} - f_{v,i+1/2}}, & f_{v,i+1/2,\max} - f_{v,i+1/2} \geq \delta \\ 0, & f_{v,i+1/2,\max} - f_{v,i+1/2} < \delta \end{cases}$$

In the breakup probability expression,

$$f_{v,i+1/2} = \left(\frac{\pi\lambda^3\sigma}{6e(\lambda)_{i+1/2}d} \right)^3. \quad (43)$$

The maximum value of the above is found by solving the expression:

$$\left(f_{v,i+1/2,\max}^{2/3} + (1 - f_{v,i+1/2,\max})^{2/3} - 1 \right) \pi d^2 \sigma = e(\lambda)_{i+1/2}. \quad (44)$$

$P_e\left(e(\lambda)_{i+\frac{1}{2}}\right)$ is found as in Equation (33).

As for the second sub-region, $P_b(f_v|d, \lambda)$ is calculated recursively backwards from $f_{v,N} = 0.5$ to $f_{v,c}$. The upper boundary is attained from the following expression:

$$P_b(f_{v,N}|d, \lambda) \quad (45)$$

$$= \begin{cases} \int_{e(\lambda)_N}^{e(\lambda)_{\text{cutoff}}} P_b(f_v|d, e(\lambda), \lambda) P_e(e(\lambda)) de(\lambda), & e(\lambda)_N < e(\lambda)_{\text{cutoff}} \\ 0, & e(\lambda)_N \geq e(\lambda)_{\text{cutoff}} \end{cases}$$

where N is the total number of iterations in both regions. The following iterations are then found by the relation:

$$\begin{aligned}
P_b(f_{v,i-1}|d, \lambda) &= \int_{e(\lambda)_{i-1}}^{e(\lambda)_{\text{cutoff}}} P_b(f_v|d, e(\lambda), \lambda) P_e(e(\lambda)) de(\lambda) \\
&= \int_{e(\lambda)_{i-1}}^{e(\lambda)_i} P_b(f_v|d, e(\lambda), \lambda) P_e(e(\lambda)) de(\lambda) \\
&\quad + \int_{e(\lambda)_i}^{e(\lambda)_{\text{cutoff}}} P_b(f_v|d, e(\lambda), \lambda) P_e(e(\lambda)) de(\lambda) \\
&\approx (e(\lambda)_i - e(\lambda)_{i-1}) P_b\left(f_{v,i-\frac{1}{2}} \middle| d, e(\lambda)_{i-\frac{1}{2}}, \lambda\right) \times P_e\left(e(\lambda)_{i-\frac{1}{2}}\right) \\
&\quad + P_b(f_{v,i}|d, \lambda)
\end{aligned} \tag{46}$$

In the above expression, $e(\lambda)_i$ is found according to:

$$e(\lambda)_i = \left(f_{v,i}^{2/3} + (1 - f_{v,i})^{2/3} - 1\right) \pi d^2 \sigma \tag{47}$$

and:

$$e(\lambda)_{i-1/2} = \frac{(e(\lambda)_i + e(\lambda)_{i-1})}{2} \tag{48}$$

As for the value of the breakup probability, it is obtained according to:

$$\begin{aligned}
P_b(f_{v,i-1/2}|d, e(\lambda)_{i-1/2}, \lambda) & \\
&= \begin{cases} \frac{1}{f_{v,i-1/2} - f_{v,i-1/2,\text{min}}}, & f_{v,i-1/2} - f_{v,i-1/2,\text{min}} \geq \delta \\ 0, & f_{v,i-1/2} - f_{v,i-1/2,\text{min}} < \delta \end{cases}
\end{aligned} \tag{49}$$

In the breakup probability expression, $f_{v,i-1/2}$ is found by solving the following equation:

$$\left(f_{v,i-1/2}^{2/3} + (1 - f_{v,i-1/2})^{2/3} - 1\right) \pi d^2 \sigma = e(\lambda)_{i-1/2} \tag{50}$$

The minimum value of the above is found using:

$$f_{v,i-1/2,\min} = \left(\frac{\pi\lambda^3\sigma}{6e(\lambda)_{i-1/2}d} \right)^3. \quad (51)$$

$P_e \left(e(\lambda)_{i-\frac{1}{2}} \right)$ is found as in Equation (33).

Implementing the above algorithm, it can be noted that a root-finding algorithm is needed in every iteration for each of the elements of both regions. Furthermore, another root-finding algorithm is needed to find f_{vc} before the f_v domain is split. This is further accentuated by the fact that the above-described algorithm should be repeated for every combination of mother-drop diameter and eddy size to account for the remaining integrations in Equation (34). The proliferated number of root-finding algorithms, as well as the numerous other iterative calculations involved, such as those of Equations (41) and (48), result in lengthy computation time before a solution can be attained. To reduce the computational effort involved in finding a solution to the PBE, this work refers to the improvements to the above algorithm proposed by Razzaghi and Shahraki (2011).

Razzaghi and Shahraki (2011) propose a robust algorithm for the calculation of the breakage frequency using the kernels of Wang et al. (2003, 2005a), following the initial algorithm put forth by Wang et al. (2004). They do this by implementing changes at the level of the probability density to reduce the number of calculations and root-finding algorithms required overall. Following a similar discretization of the f_v domain, and using the same lower boundary condition and value of first iteration, the probability density is found iteratively forward in the first region, $f_v \in [0, f_{vc}]$, according to the following altered approximation:

$$\begin{aligned}
P_b(f_{v,i+1}|d, \lambda) &= \int_{e(\lambda)_{i+1}}^{e(\lambda)_{\text{cutoff}}} P_b(f_v|d, e(\lambda), \lambda) P_e(e(\lambda)) de(\lambda) \\
&= \int_{e(\lambda)_{i+1}}^{e(\lambda)_i} P_b(f_v|d, e(\lambda), \lambda) P_e(e(\lambda)) de(\lambda) \\
&\quad + \int_{e(\lambda)_i}^{e(\lambda)_{\text{cutoff}}} P_b(f_v|d, e(\lambda), \lambda) P_e(e(\lambda)) de(\lambda) \\
&\approx \frac{1}{2} (e(\lambda)_i - e(\lambda)_{i+1}) \{P_b(f_{v,i}|d, e(\lambda)_i, \lambda) P_e(e(\lambda)_i) \\
&\quad + P_b(f_{v,i+1}|d, e(\lambda)_{i+1}, \lambda) P_e(e(\lambda)_{i+1})\} + P_b(f_{v,i}|d, \lambda).
\end{aligned} \tag{52}$$

In the above expression, $e(\lambda)_i$ is found according to:

$$e(\lambda)_i = \frac{\pi \lambda^3 \sigma}{6 f_{v,i}^{1/3} d}. \tag{53}$$

As for the value of the breakup probability above, it is obtained according to:

$$P_b(f_{v,i}|d, e(\lambda)_i, \lambda) = \begin{cases} \frac{1}{f_{v,i,\text{max}} - f_{v,i}}, & f_{v,i,\text{max}} - f_{v,i} \geq \delta \\ 0, & f_{v,i,\text{max}} - f_{v,i} < \delta \end{cases} \tag{54}$$

The maximum breakup fraction used in the above expression is found by solving:

$$\left(f_{v,\text{max}}^{2/3} + (1 - f_{v,\text{max}})^{2/3} - 1 \right) \pi d^2 \sigma = e(\lambda) \tag{55}$$

$P_e(e(\lambda)_i)$ is found as in Equation (28).

As for the second sub-region, $P_b(f_v|d, \lambda)$ is similarly calculated recursively backwards from $f_{v,N} = 0.5$ to $f_{v,c}$, using the same upper boundary condition as in the Wang et al. (2004) algorithm. The following iterations are then found by the altered relation:

$$\begin{aligned}
P_b(f_{v,i-1}|d, \lambda) &= \int_{e(\lambda)_{i-1}}^{e(\lambda)_{\text{cutoff}}} P_b(f_v|d, e(\lambda), \lambda) P_e(e(\lambda)) de(\lambda) \\
&= \int_{e(\lambda)_{i-1}}^{e(\lambda)_i} P_b(f_v|d, e(\lambda), \lambda) P_e(e(\lambda)) de(\lambda) \\
&\quad + \int_{e(\lambda)_i}^{e(\lambda)_{\text{cutoff}}} P_b(f_v|d, e(\lambda), \lambda) P_e(e(\lambda)) de(\lambda) \\
&\approx \frac{1}{2} (e(\lambda)_i - e(\lambda)_{i-1}) \{P_b(f_{v,i-1}|d, e(\lambda)_{i-1}, \lambda) P_e(e(\lambda)_{i-1}) \\
&\quad + P_b(f_{v,i}|d, e(\lambda)_i, \lambda) P_e(e(\lambda)_i)\} + P_b(f_{v,i}|d, \lambda)
\end{aligned} \tag{56}$$

In the above expression, $e(\lambda)_i$ is found according to:

$$e(\lambda)_i = \left(f_{v,i}^{2/3} + (1 - f_{v,i})^{2/3} - 1 \right) \pi d^2 \sigma \tag{57}$$

As for the value of the breakup probability above, it is obtained according to:

$$P_b(f_{v,i}|d, e(\lambda)_i, \lambda) = \begin{cases} \frac{1}{f_{v,i} - f_{v,i,\min}}, & f_{v,i} - f_{v,i,\min} \geq \delta \\ 0, & f_{v,i} - f_{v,i,\min} < \delta \end{cases} \tag{58}$$

The minimum breakup fraction used in the above expression is found as:

$$f_{v,i,\min} = \left(\frac{\pi \lambda^3 \sigma}{6e(\lambda)_i d} \right)^3 \tag{59}$$

$P_e(e(\lambda)_i)$ is found as in Equation (33).

The alterations in the above algorithm can be seen to reduce the number of root-finding algorithms and iterative calculations required. Each of the iterations of the first sub-region of the domain requires one root-finding algorithm, in addition to the one needed to find f_{vc} . However, the second sub-region is completely free of any root-finding algorithms, and has considerably fewer calculations. These significantly contribute to the reduction in computation time.

4.2. Results and Validation

4.2.1. Numerical Findings on the Optimization of Coefficients

Following the application of the optimization method, the results were tabulated and graphed for each of the optimizations, as described above, and for each of the studied PBE cases. The values for the obtained optimized breakage and coalescence constants are tabulated below.

Model Parameter \ SDS Concentration	0 ppm	2 ppm	5 ppm	10 ppm
C_1	3.0933	0.31675	0.20075	0.3942
C_2	4.7812	0.58004	0.16217	0.86426
C_3	1.3068×10^{-1}	0.59502×10^{-1}	0.3846×10^{-1}	0.23749×10^{-1}
C_4	$2.3 \times 10^{12} \text{ m}^{-2}$	$1 \times 10^{10} \text{ m}^{-2}$	$1 \times 10^{10} \text{ m}^{-2}$	$1 \times 10^{10} \text{ m}^{-2}$

Table 1: Optimized values of the breakage and coalescence parameters for surfactant concentrations $C_{\text{SDS}} = 0 \text{ ppm}$, $C_{\text{SDS}} = 2 \text{ ppm}$, $C_{\text{SDS}} = 5 \text{ ppm}$, $C_{\text{SDS}} = 10 \text{ ppm}$

For zero SDS concentration and 7% dispersed phase holdup, the resultant calculated Sauter mean diameters using the optimized values of the breakage and coalescence coefficients were graphed against the distance along the pipe, along with the experimentally obtained values of the Sauter mean diameter, for each of the studied flow speeds. The results were as follows:

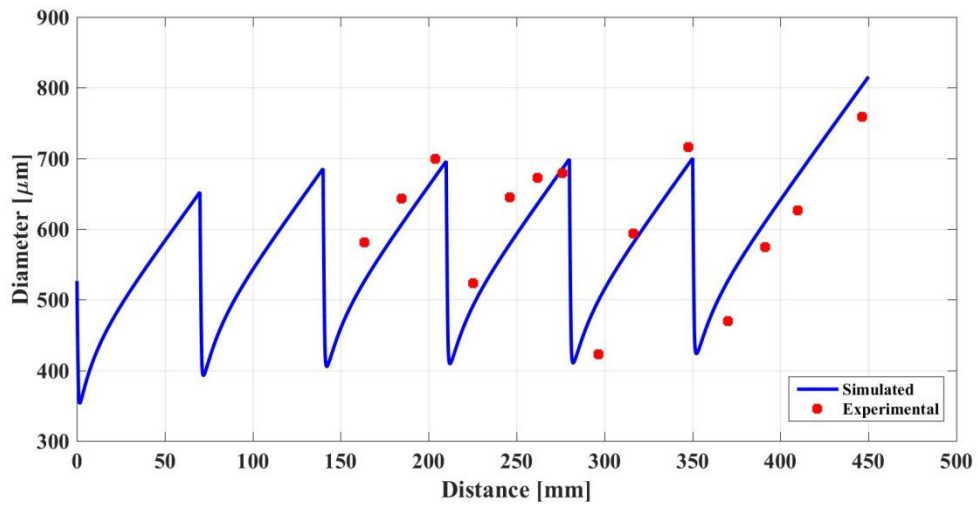


Figure 2: The spatial variation of the calculated Sauter mean diameter along the reactor/contact length ($U = 1.3 \text{ m/s}$, $\Phi = 7\%$, $C_{\text{SDS}} = 0 \text{ ppm}$) with the corresponding experimentally measured values of the Sauter mean diameter

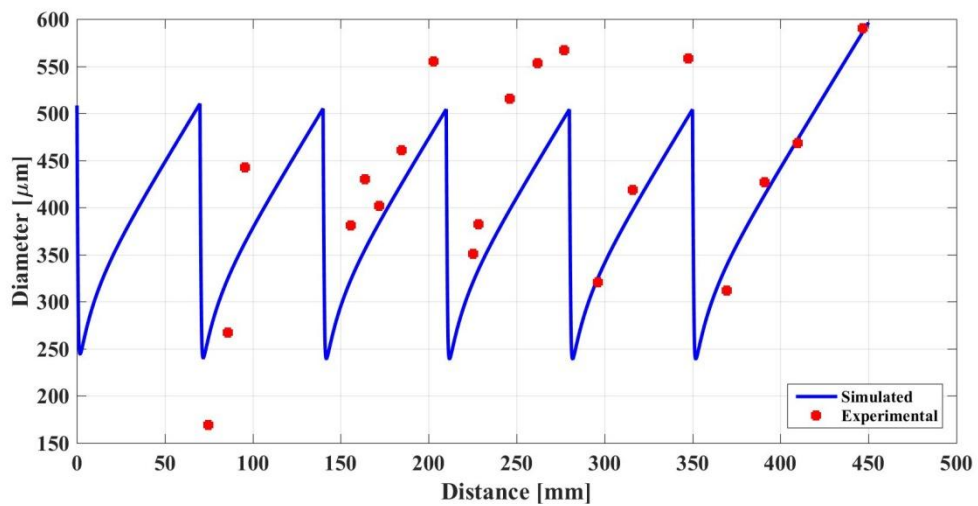


Figure 3: The spatial variation of the calculated Sauter mean diameter along the reactor/contactor length ($U = 2 \text{ m/s}$, $\Phi = 7\%$, $C_{\text{SDS}} = 0 \text{ ppm}$) with the corresponding experimentally measured values of the Sauter mean diameter

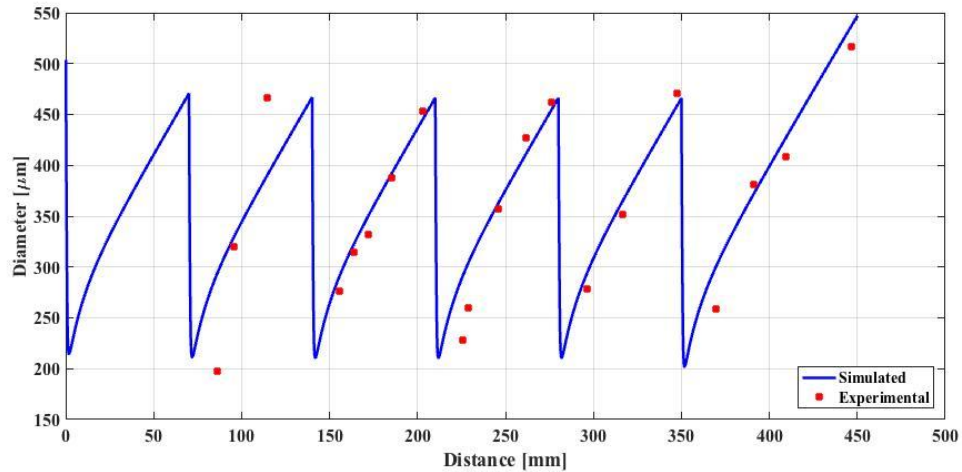


Figure 4: The spatial variation of the calculated Sauter mean diameter along the reactor/contactor length ($U = 2.3 \text{ m/s}$, $\Phi = 7\%$, $C_{\text{SDS}} = 0 \text{ ppm}$) with the corresponding experimentally measured values of the Sauter mean diameter

Figures 2, 3, and 4 show the axial variation of the Sauter mean diameter along the length of the reactor after optimizing the various model constants under the experimental conditions specific to Figure 2. As the simulated Sauter mean diameters depend on the model constants using the kernels of Coulaloglou and Tavlarides (1977), the plots reflect the accuracy of the obtained constants and the optimization method. The hydrodynamic conditions depicted in Figure 2 can be considered as typical for those experimentally investigated, and the values of the model constants derived thereof

should be independent of the operating conditions and design parameters of the mixer (Azizi and Al Taweel, 2007). This is clearly portrayed in Figures 3 and 4 when the hydrodynamic conditions, namely holdup and flow speed, are changed, but the simulated Sauter means still give accurate predictions along the pipe for the model constants obtained for the conditions of Figure 2.

On the other hand, varying the surfactant concentration in the system was found to affect the values of the model constants (Table 1). By changing the SDS concentrations to 2 ppm, 5 ppm, and 10 ppm, the non-linear optimization algorithm gave different results for each, which were in turn different from the model constant values obtained for SDS concentration of 0 ppm. The constants obtained for each SDS concentration gave accurate predictions for various flow speeds.

For surfactant concentration $C_{\text{SDS}} = 2$ ppm, and 7% dispersed phase holdup, the resultant calculated Sauter mean diameters using the optimized values of the breakage and coalescence coefficients were graphed along with the experimentally obtained values of the Sauter mean diameter for a flow speed of 2 m/s. The results were as follows:

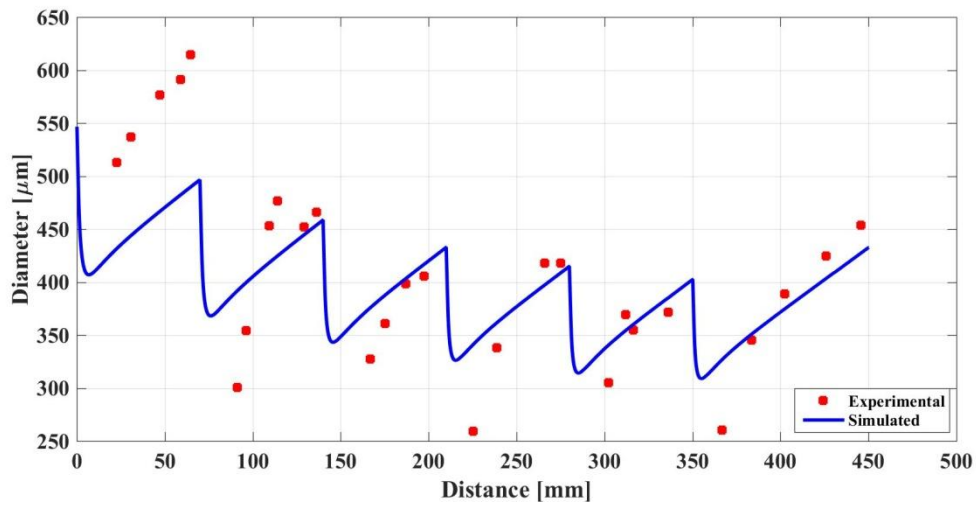


Figure 5: The spatial variation of the calculated Sauter mean diameter along the reactor/contacter length ($U = 2 \text{ m/s}$, $\Phi = 7\%$, $C_{\text{SDS}} = 2 \text{ ppm}$) with the corresponding experimentally measured values of the Sauter mean diameter

Figure 5 clearly shows the impact which surfactants have on the bubble breakage and coalescence processes when added to the multi-phase system. This can be seen by monitoring the axial variation of the Sauter mean diameter as the two-fluid dispersion passes through the consecutive high energy dissipation regions generated by the screens positioned every 70 mm, and comparing it to the variation in a similar system with zero surfactant concentration (Figure 3). Although the model of Coualoglou and Tavlarides (1977) did not accurately predict the first two stages, it accurately predicted the spatial variation of the Sauter mean diameter throughout the remainder of the contactor. This difficulty is most probably caused by the fact that this model takes into account neither the effect of interfacial elasticity nor bubble breakage by cutting action, a mechanism that is expected to play a large role when the bubbles are much bigger than the screen mesh size. The tendency of bubbles to shed micro-bubbles

in the presence of surfactants could also have contributed to the deviation (Azizi and Al Taweel, 2007). With the increase of the surfactant concentration added to the system from 2 ppm to 5 ppm and 10 ppm, similar conclusions can be made from the results (Figures 6 and 7).

For surfactant concentration $C_{SDS}=5$ ppm, and 7% dispersed phase holdup, the resultant calculated Sauter mean diameters using the optimized values of the breakage and coalescence coefficients were graphed along with the experimentally obtained values of the Sauter mean diameter for a flow speed of 2 m/s. The results were as follows:

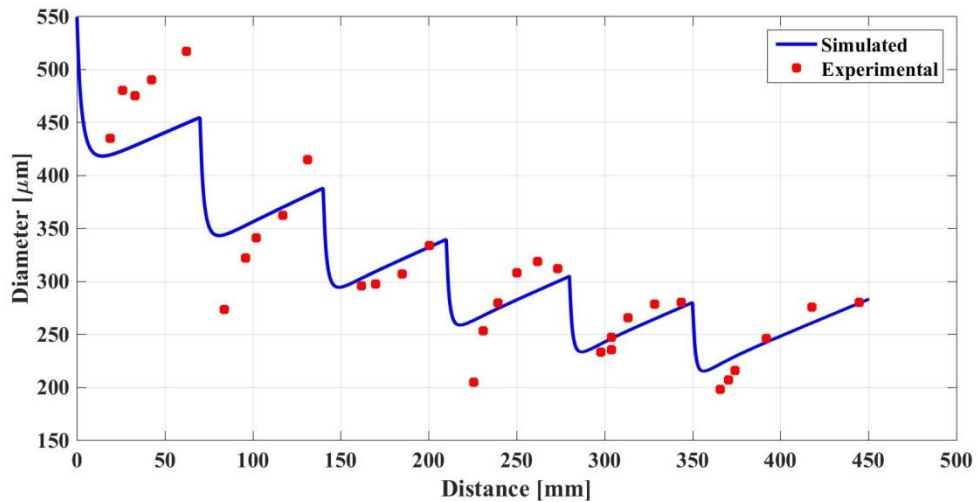


Figure 6: The spatial variation of the calculated Sauter mean diameter along the reactor/contactator length ($U = 2$ m/s, $\Phi = 7\%$, $C_{SDS} = 5$ ppm) with the corresponding experimentally measured values of the Sauter mean diameter

For surfactant concentration $C_{SDS}=10$ ppm, and 7% dispersed phase holdup, the resultant calculated Sauter mean diameters using the optimized values of the breakage and coalescence coefficients were graphed along with the experimentally obtained values of the Sauter mean diameter for a flow speed of 2 m/s. The results were as follows:

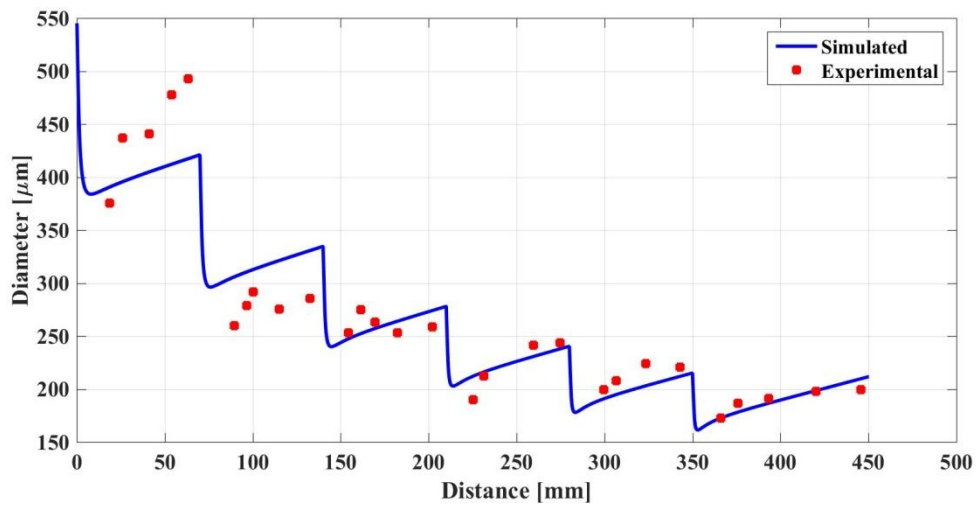


Figure 7: The spatial variation of the calculated Sauter mean diameter along the reactor/contacter length ($U = 2$ m/s, $\Phi = 7\%$, $C_{SDS} = 10$ ppm) with the experimentally measured values of the Sauter mean diameter

As can be seen from Figure 8 below, the model well-predicts the effect of surfactants on the average Sauter mean diameter. However, it under-predicts the effect of surfactant concentration in the case of lower velocities (1.3 m/s), a situation that is most probably caused by the fact that interfacial elasticity is known to increase with increasing surfactant concentration within the concentration range investigated, and that

within the surface ages encountered during bubble collisions (order of milliseconds) the elasticity is essentially a linear function of the surface age (Azizi and Al Taweel, 2007). As the surfactant concentration increases, the average bubble diameter, or Sauter mean diameter, decreases in a similar way for various flow speeds.

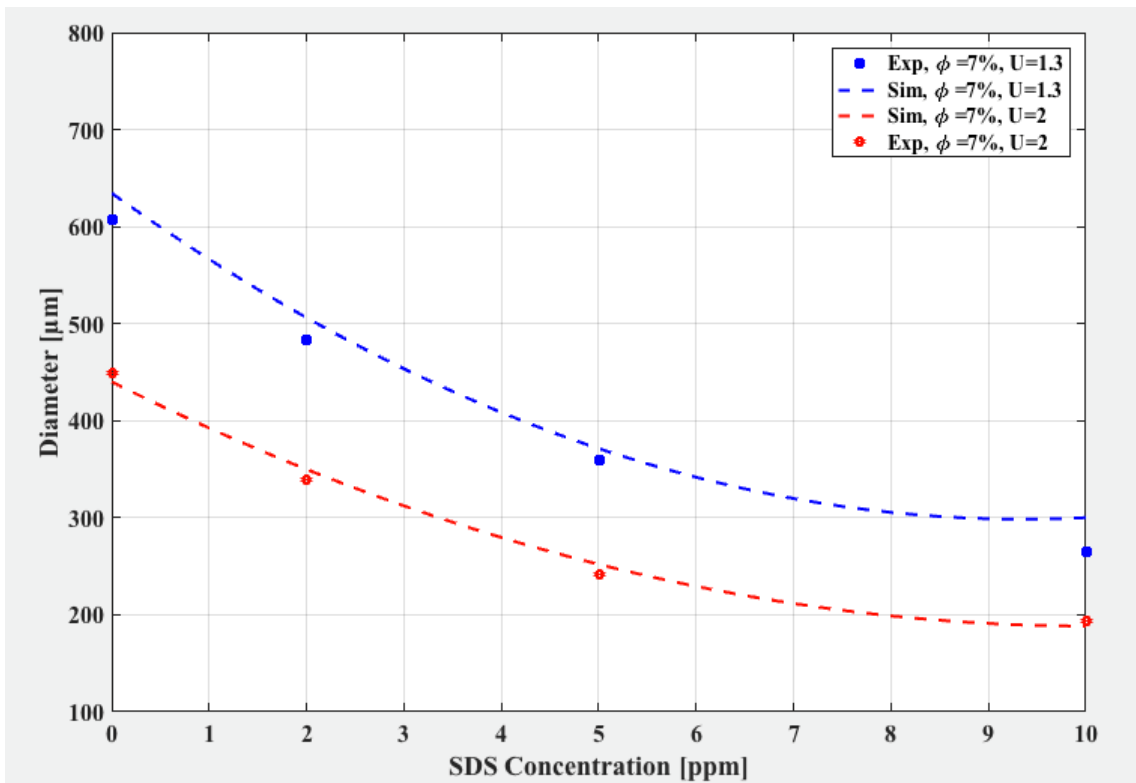


Figure 8: Effect of SDS concentration on the average Sauter mean diameter in the 6th stage of the pipe

Figure 9 clearly depicts the effect of changing the operating conditions on the Sauter mean diameter prevalent through stage 6, where quasi-steady state conditions are considered to be reached. Accordingly, the average equilibrium diameter was found to

decrease with increasing superficial velocity. This is mainly due to the enhanced energy dissipation rates in the regions downstream of the screens which, in turn, result in increasing bubble breakage rates. The higher average energy dissipation levels encountered further downstream result in higher coalescence rates, but the net effect is that of finer bubble generation, particularly in the presence of surfactants which retard coalescence. However, the effect of increasing gas holdup (or gas-to-liquid flow ratios) shows an opposite trend where the average bubble diameter clearly increases as the gas holdup in raised from 1% to 7%. This is mainly caused by the larger bubble population densities encountered at higher gas holdups and the subsequent increase in bubble collision and coalescence rates (Azizi and Al Taweel, 2007).

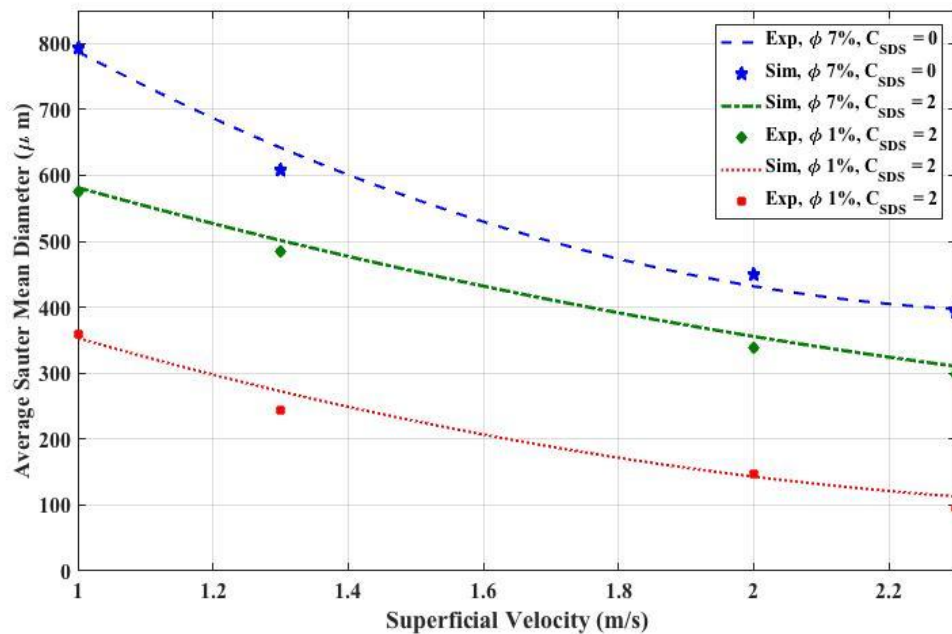


Figure 9: Effect of varying the superficial velocity and holdup on the equilibrium Sauter mean diameter in stage 6

As can be seen from Figure 9, the breakage and coalescence models of Coualoglou and Tavlarides (1977), used in this part of the investigation, can accurately predict the effect of varying some hydrodynamic conditions, namely gas holdup, residence time, and local turbulence intensities, on the Sauter mean diameter.

4.2.2. Wang Model

The kernels of the Wang et al. model were incorporated in the birth by breakage, death by breakage, birth by coalescence, and death by coalescence sub-processes of the PBE. Each sub-process was studied individually, then their sum was used to solve the overall PBE. The computational domains of the integrals of the birth and death by coalescence rates, as well as the birth by breakage rate, were divided into 60-element finite difference meshes.

4.2.2.1. Coalescence Sub-Processes

4.2.2.1.1. Birth by Coalescence

The birth by coalescence sub-processes yielded smooth results for the given discretization and numerical solution method for various values of energy dissipation throughout the simulated pipe equipped with static mixers.

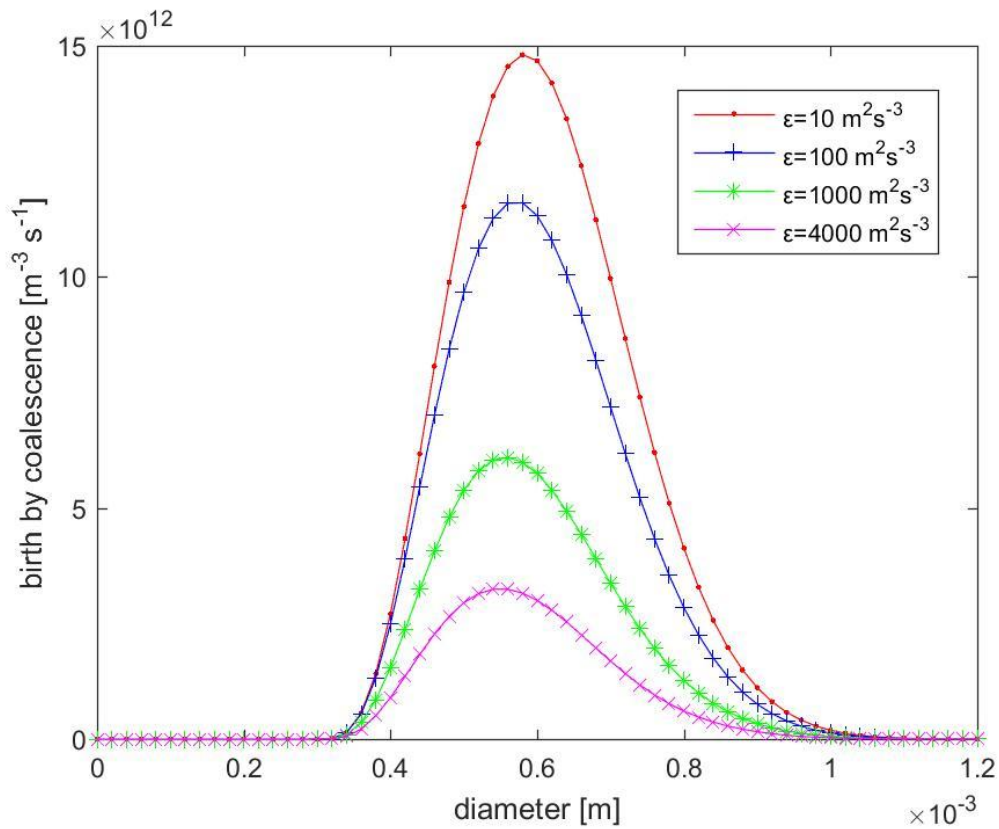


Figure 10: Typical curves for the birth by coalescence rate at typical diameter values in the system for energy dissipation rates of $10 \text{ m}^2 \text{ s}^{-3}$, $100 \text{ m}^2 \text{ s}^{-3}$, $1000 \text{ m}^2 \text{ s}^{-3}$, and $4000 \text{ m}^2 \text{ s}^{-3}$

The representations are accurate as the bubbles generated from coalescence are not the smallest ones, rather the curve is shifted towards the middle and large sized bubbles. On the other hand, the curves show almost no generation of the largest, unstable, bubbles.

4.2.2.1.2. Death by Coalescence

The death by coalescence sub-process simulation also yielded a stable solution throughout the various energy dissipation regions of the given pipe. The results in Figure 11 show a higher death rate for smaller bubbles, which readily coalesce together, with a lower death rate for the larger ones, which rarely coalesce. This is due to the fact that the larger a bubble gets, the more unstable it becomes, hence the tendency of bubbles to remain under a certain size.

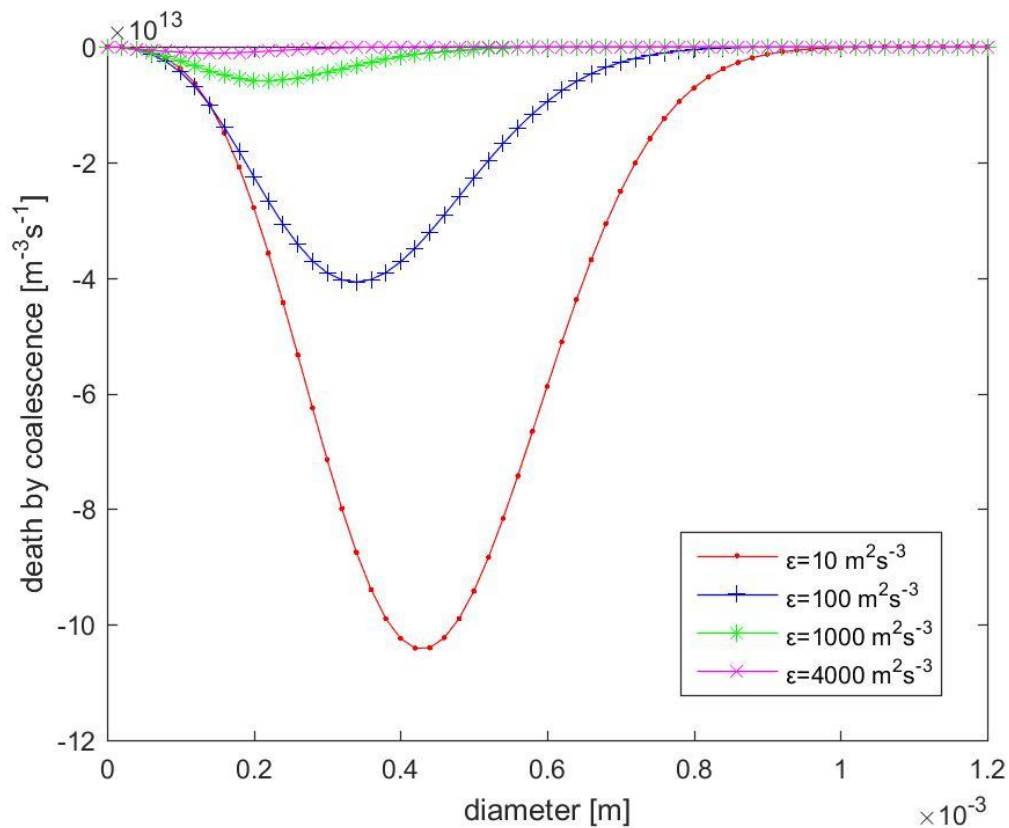


Figure 11: Typical curves for the death by coalescence rate at typical diameter values in the system for energy dissipation rates of $10 \text{ m}^2\text{s}^{-3}$, $100 \text{ m}^2\text{s}^{-3}$, $1000 \text{ m}^2\text{s}^{-3}$, and $4000 \text{ m}^2\text{s}^{-3}$

This term can be seen to have a higher magnitude than that of the birth by coalescence term. This is primarily due to the fact that more than one bubble must coalesce together to form one resultant bubble. Hence, more than one “death” are required for one “birth”. The death by coalescence rates can be compared to the birth by coalescence rates for various energy dissipation rates in Figure 12 below.

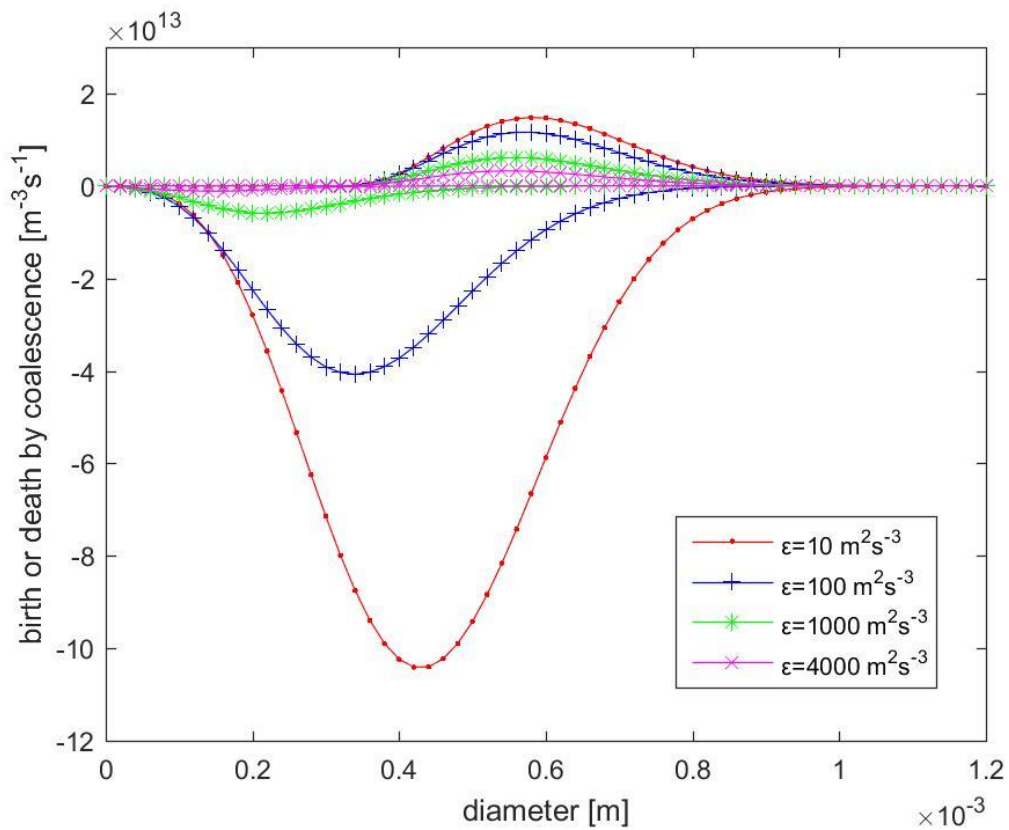


Figure 12: The birth by coalescence rates (positive) and the death by coalescence rates (negative) for typical diameter values in the system at energy dissipation rates of $10 \text{ m}^2\text{s}^{-3}$, $100 \text{ m}^2\text{s}^{-3}$, $1000 \text{ m}^2\text{s}^{-3}$, and $4000 \text{ m}^2\text{s}^{-3}$

4.2.2.2. Breakage Sub-Processes

4.2.2.2.1. Birth by Breakage

Similarly to the coalescence terms, the birth by breakage term also yielded a smooth result for varying energy dissipation for the given discretizations and numerical integration method. This term is generally larger than the death by breakage term as one breaking bubble yields two or more daughter bubbles.

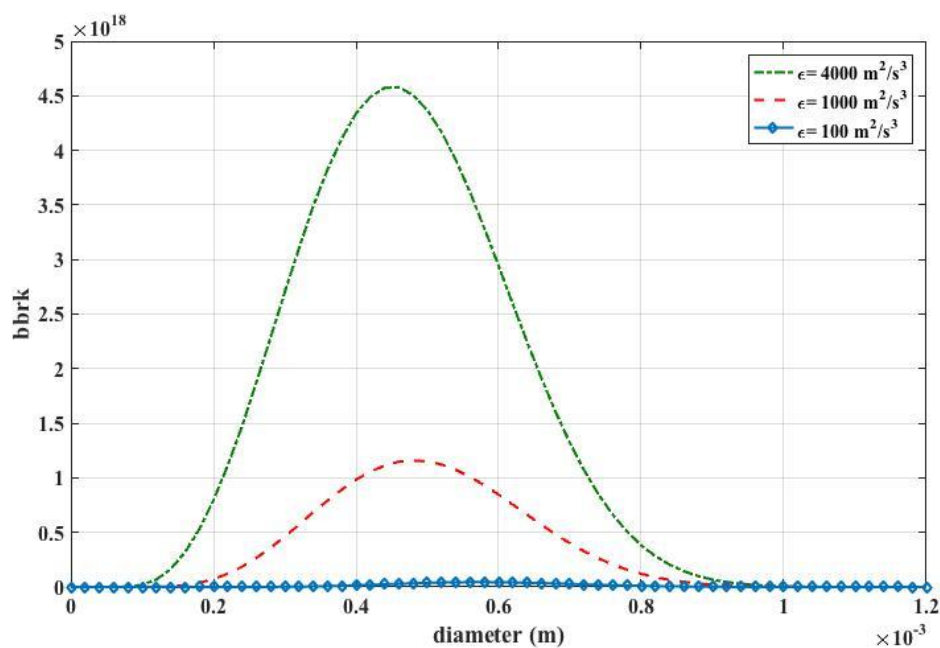


Figure 13: Typical curves for birth by breakage rate at typical diameters in the system for energy dissipation rates of $100 \text{ m}^2\text{s}^{-3}$, $1000 \text{ m}^2\text{s}^{-3}$, and $4000 \text{ m}^2\text{s}^{-3}$

The resultant graphs show that smaller bubbles are more profoundly created by breakage than larger bubbles, which is physically correct. Conversely, larger bubbles are rarely created by breakage, as can be seen in the numerical representations.

4.2.2.2.2. Death by Breakage

Contrastingly to the above sub-processes, the death by breakage term was found to yield fluctuations at the regions of highest turbulence just after the screens within the pipe. This is traced back to the breakage rate/frequency kernel which only has an effect on the numerical solution of this particular sub-process.

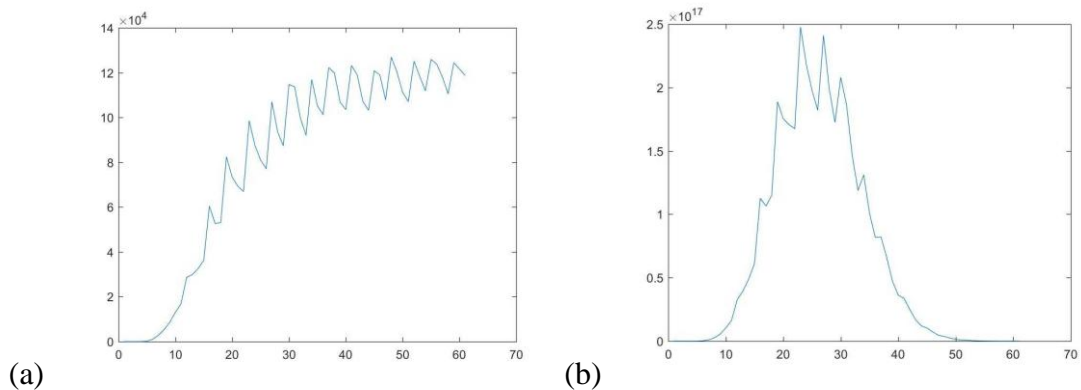


Figure 14: The breakage frequency (a) and the corresponding death by breakage rate (b) over the diameter sample points for a twice-as-fine discretization of the energy domain

These numerical fluctuations are resolved by taking a finer discretization of the energy domain, or turbulent eddy lengths, involved in the integral of the breakage frequency/rate. However, to avoid unnecessary refinement resulting in an ineffective

increase in computation time, such discretization should not be uniform within the pipe. In this work, regions of high energy dissipation were refined, while those with moderate or low energy dissipations were left with similar discretizations to those used to represent the above sub-processes.

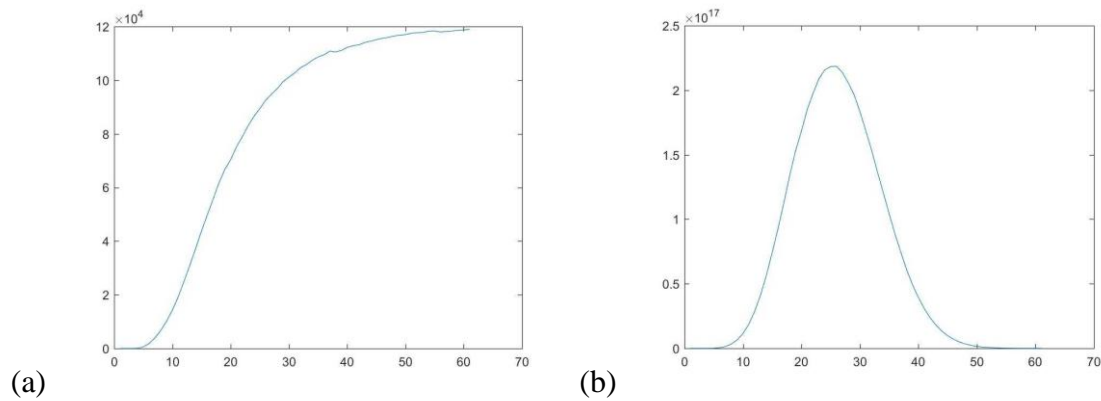


Figure 15: The breakage frequency (a) and the corresponding death by breakage rate (b) over the diameter sample points for a 50-times-as-fine discretization of the energy domain

As can be seen, the finer the finite difference is in regions of high energy dissipation, the more stable the solution becomes. Even 50-fold discretization yields some numerical instabilities in the larger diameter regions, thus showing a need for even finer discretization. However, the more stable solutions show accordance with physical observation as a higher death by breakage rate exists for larger bubbles, while smaller bubbles break less often.

4.2.2.3. Solution of the Population Balance Equation

Summing together the spatially variant solutions of the above four sub-processes yields the spatial solution of the population balance equation throughout the pipe. Here, spatial variation also refers to energy dissipation variation, as there is a static mixer situated periodically (lengthwise) in the studied pipe.

In order to represent the solution, avoiding the lengthy computation time resulting from the extreme refinement of the high energy dissipation regions, the represented energy dissipation was taken to be 1% of the actual energy dissipation in the pipe in the following figure.

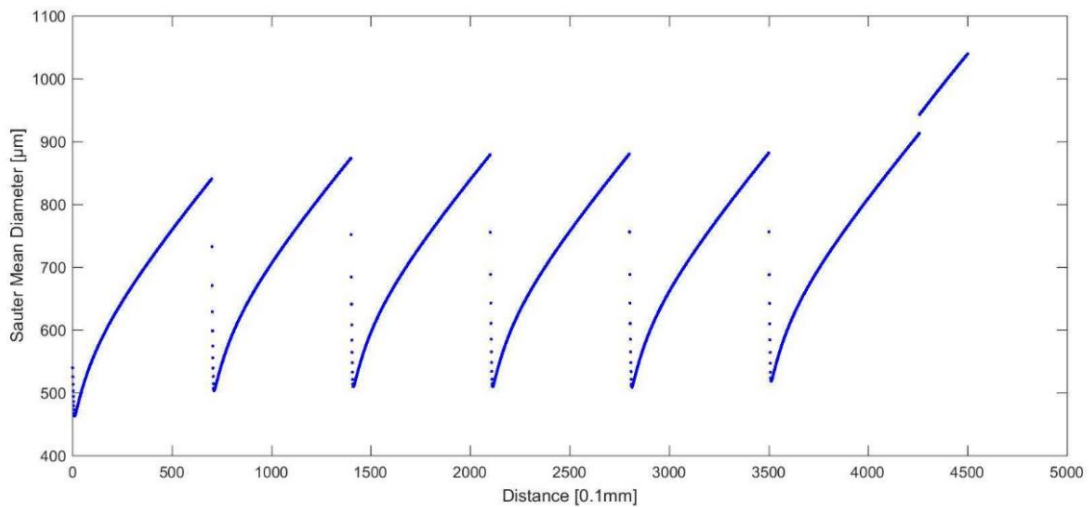


Figure 16: The overall solution of the PBE at reduced energy dissipation along the pipe

Taking the actual energy dissipation rates, but with moderate energy domain refinement by dividing each division by 10, the population balance equation yielded a

highly fluctuating solution with severe instability. However, with greater refinement, dividing each division by 50, a similar solution shape to the low energy simulation was obtained. The Sauter mean diameters obtained were more accurate, however some fluctuation could still be seen in the regions of highest energy dissipation following the screens. The greater accuracy comes at a cost of greater computation time.

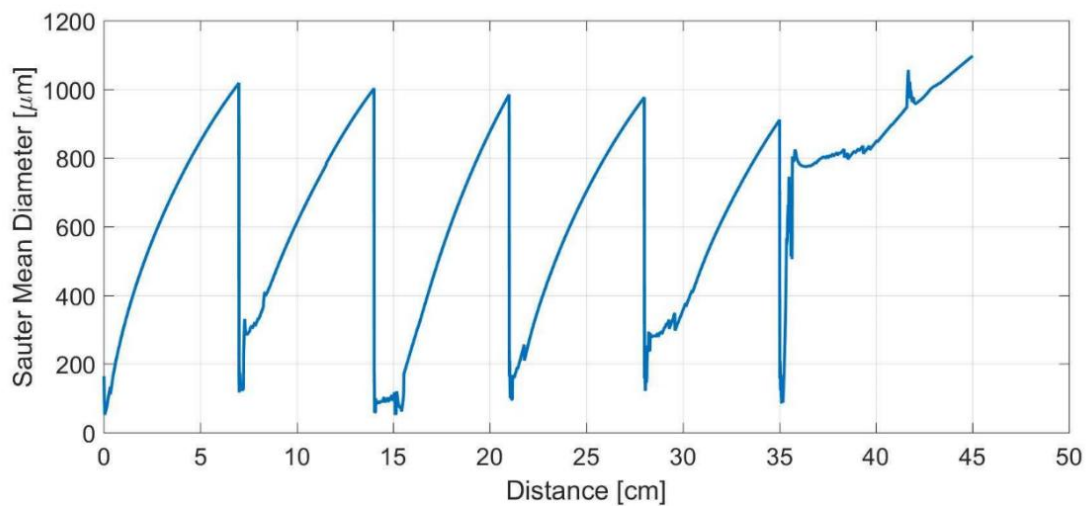


Figure 17: The overall solution of the PBE at 50-fold discretization of the energy domain

4.3. Discussion

In both parts of the above work, the optimization part and the Wang model part, the numerical errors arise from several sources, differing in impact. First of all, there are round off errors which occur because the machine used for simulation cannot take only take a certain number of decimals while the numbers may require a longer representation. In this case, the actual values are truncated. Secondly, the finite domain

errors, which result from representing an infinite internal coordinate by a finite value, also contribute to the deviation. Thirdly, the mathematical models themselves are only approximations of what is happening in the system, and cannot faultlessly represent reality. Furthermore, the methods used for integration and root-finding involved in the solution are approximations with finite user-defined precisions. Finally, imprecision also arises from the domain discretizations involved in the finite difference method used in the above-described solution method. These errors are magnified when combined, and are further increased in the iterative calculations where the approximations of a previous iteration are used as input for the following iteration which in turn adds to the deviations before moving on to the following iteration. However, the overall errors in the above study are normal, unavoidable, yet acceptable at the applied macro scale. Nonetheless, there is much room for improvement. Higher accuracy can be obtained through cumulative refinements in further studies, especially when coupled with the prospected continuous improvements in computation technology.

CHAPTER 5

CONCLUSION AND RECOMMENDATIONS

5.1. Conclusion

The above work consisted of simulating a multi-phase flow in a 45 cm pipe equipped with screen-type static mixers at 7 cm intervals from the start of the pipe. In this system, each screen is followed by a region of high turbulence, which is in turn followed by regions of moderate then low turbulence. Gas-liquid flow was specifically considered, both with and without the presence of surfactants in the medium. This setup was used to optimize the coefficients of the model of Coualoglou and Tavlarides (1977) for dispersed phase breakup and coalescence in gas-liquid flow. The same setup was used to study the applicability of the model of Wang et al. (2003, 2005a) to such systems.

5.1.1. Optimization of Coefficients

Following the implementation of the Levenberg-Marquardt optimization algorithm, and after formulating the sum of least-square function to be used therein, for the multitude of studied SDS concentrations, the non-linear minimum finding approach was found to yield good results. Even when the optimized coefficients of each SDS case were used to generate the Sauter mean diameter throughout the static-screen mixer pipe, for different flow conditions (i.e., different flow speeds and gas holdups), the simulated values were found to conform with the experimental results to an agreeable extent.

These coefficient values differed from one SDS case to another, and differed from the values available in the literature, due to the specificity of the studied cases. These constants were found to be highly dependent on the flow composition. Out of the four constants, the coalescence efficiency constant, C_4 , was found to have the greatest value by over 10 degrees of magnitude compared to the others, with little effect of changing its value. Therefore, it was set to be fixed during the optimizations to ensure the precision of predicting the remaining constants, and to decrease the required computation time.

5.1.2. Wang et al. (2003, 2005a) Model Implementation

After compiling the complete models of Wang et al. (2003, 2005a) for breakage and coalescence of bubbles in multiphase flow, the implementation was comprised of several steps. First of all, the coalescence kernels were clearly formulated in themselves. However, the integrals which use these kernels to find the coalescence birth and death rates were written in terms of volume, as opposed to the kernels which were written in terms of bubble diameters. Correspondingly, a suitable adjustment of variables was undergone, after which the integral domains were discretized into meshes of 60 finite difference elements. The trapezoidal method was implemented to solve these integrals, yielding stable numerical results for the given discretizations.

The breakage kernels were then formulated, but the work was less simple. The birth by breakage term, which involves a triple integral which is then integrated to obtain the birth by breakage rate, thus yielding a quadruple integral, required immense computation time. This could not be resolved through parallelization, as the

discretizations of the various integral domains were interdependent. Thus, to overcome this issue, a reduction of the number of integrals was implemented by resorting to the algorithms of Wang et al. (2004) and Razzaghi and Shahraki (2011). This step reduced the inner triple integral to a double one and reduced the overall number of calculations within the integrals, resulting in a reduction of computation time. Furthermore, the same triple integral is used in the death by breakage term. To avoid recalculation, the values were saved in matrix form from the birth by breakage solution, to be readily fed back into the program without any calculations for the death by breakage term.

Besides the number of integrals and calculations, the death by breakage term faced a further complication when calculated for high energy dissipation rates. The higher the energy dissipation, the more numerous the turbulent eddies in the studied flow, and hence the smaller they become. In the Wang et al. coalescence terms, the integrals have no dependence on the energy domain, and so the discretizations are independent of the turbulence intensity. Their stability is hence unaffected by the change of energy dissipation rate. Similarly, the stability of the birth by breakage term is also independent of the energy domain discretization as the dependent terms are cancelled out due to the simplifications within. However, the death by breakage term alone is dependent on this domain, specifically in the outer integral of the breakage rate/frequency term. Instabilities were found to occur for high energy dissipation rates coupled with the 60-element finite difference discretizations used for the other terms. However, when these meshes were slightly refined, the solution became smoother. Further refinement resulted in relatively stable solutions, but at the expense of computation time. A linear increase in mesh refinement resulted in a geometric increase in computation time as a result of nested integration.

As the final solution of the population balance equation (PBE) depends on the summation of the solutions of the birth by breakage, death by breakage, birth by coalescence, and death by coalescence terms, an instability in one will result in instability in the overall solution. Hence, a stable solution of the PBE was found to depend on the extent on discretization of the energy domain, or eddy lengths, in regions of high energy dissipation rates (to the order of $10^3 \text{ m}^2\text{s}^{-3}$) just after the static screen mixers in the studied pipe. In the lower energy dissipation regions, the solution was found to be stable under the common discretization of 60 finite difference elements per integral domain. To maintain stability in regions of high energy dissipation, the eddy length domain required discretizations over 50 times as fine.

5.2. Recommendations

5.2.1. Optimization of Coefficients

The resulting optimized values of breakage and coalescence coefficients can be used in further studies, given that the studied flow has the same chemical composition. Even a small variation in composition was found to entail a notable change in the coefficient optimal values. The values obtained in this study can be used for similar gas-liquid flows, with or without surfactants. However, in the presence of surfactants, the constants taken from this study should be those corresponding to the surfactant concentration in the studied flow. In the absence of surfactants, the constants obtained for zero SDS concentration should be used.

Furthermore, later studies have grounds for improving the current values of the constants. This can be attained by increasing the accuracy of the used optimization

method, coupled with a use of more powerful computation machines to counter the resulting increase in computation time.

Finally, the constants will differ when the nature of the mixer involved in the studied multiphase flow differs. No general set of constants can be found, for the current mathematical expressions of the coefficients, for all types of flows. Hence, to avoid the necessity of optimizing the coefficients before every different application, it is recommended that a model without adjustable coefficients is used. This has become easier with the emergence of coefficient-free breakage and coalescence models, such as those of Wang et al. (2003, 2005a), Zhao and Ge (2007) and others. However, if models with constants are found to be more physically accurate for the studied case, it is recommended that a comprehensive set of optimized coefficients, for the various possible cases of study, is generated. Such a comprehensive set may open doors for finding a trend in the way the constants vary depending on the possible changes in flow properties.

5.2.2. Wang et al. (2003, 2005a) Model Implementation

Following the observations regarding the effect of domain discretization in regions of high energy dissipation on the overall solution of the population balance equation, it is recommended that a relatively fine mesh, of about 100-fold the discretizations in the low energy dissipation regions, is taken. Furthermore, to avoid excessive needless computation, it is recommended that the studied multiphase systems are divided into 3 regions as a first step towards formulating a non-uniform mesh. The first region should account for areas of high energy dissipation rates of the order of $10^3 \text{ m}^2\text{s}^{-3}$ and above, with 100-fold, or more, discretizations. The second should be for

regions of moderate energy dissipation rates of the order of $10^2 \text{ m}^2\text{s}^{-3}$ with approximately 50-fold discretizations. The third should be for regions of relatively low energy dissipation rates, of the order of $10^1 \text{ m}^2\text{s}^{-3}$ and below, with unit discretizations. This would only increase the computation time where necessary.

On the other hand, the computation time can further be reduced by employing parallel computing. However, to do so, the algorithm used should be restructured for parallelization. Furthermore, it is recommended that a platform other than MATLAB, more specific to numerical integration, is used in future studies based on similar mathematical models with nested integrals. Overall, the computations were successfully employed, but with major complications that should be avoided in future studies.

REFERENCES

Alexopoulos, A.H., Roussos, A.I., & Kiparissides, C. (2004). Part I: Dynamic Evolution of the Particle Size Distribution in Particulate Processes Undergoing Combined Particle Growth and Aggregation. *Chemical Engineering Science*, 59(24), 5751-5769.

Alexopoulos, A.H., & Kiparissides, C.A. (2005). Part II: Dynamic Evolution of the Particle Size Distribution in Particulate Processes Undergoing Simultaneous Particle Nucleation, Growth and Aggregation. *Chemical Engineering Science*, 60(19), 4157-4169.

Alopaeus, V., Koskinen, J., & Keskinen, K.I. (1999). Simulation of the Population Balances for Liquid–Liquid Systems in a Nonideal Stirred Tank. Part 1 Description and Qualitative Validation of the Model. *Chemical Engineering Science*, 54(24), 5887-5899.

Alopaeus, V., Koskinen, J., Keskinen, K.I., & Majander, J. (2002a). Simulation of the population balances for liquid–liquid systems in a nonideal stirred tank. Part 2 Parameter Fitting and the Use of the Multiblock Model for Dense Dispersions. *Chemical Engineering Science*, 57(10), 1815-1825.

Alopaeus, V., Keskinen, K.I., Koskinen, J., & Majander, J. (2002b). Gas-Liquid Stirred Tank Reactor Modeling with CFD and User Subroutines. *A.I.Ch.E. Annual Meeting*, Indianapolis, IN, November 3-8.

Alopaeus, V., Koskinen, J., & Keskinen, K.I. (2003). Utilization of Population Balances in Simulation of Liquid-Liquid Systems in Mixed Tanks. *Chemical Engineering Communications*, 190(11), 1468-1484.

- Alopaeus, V., Laakkonen, M., & Aittamaa, J. (2006). Numerical Solution of Moment-Transformed Population Balance Equation with Fixed Quadrature Points. *Chemical Engineering Science*, *61*(15), 4919-4929.
- Al Taweel, A.M., Li, C., Gomaa, H.G., & Yuet, P. (2007). Intensifying Mass Transfer between Immiscible Liquids: Using Screen-type Static Mixers. *Chemical Engineering Research and Design*, *85*(5), 760-765.
- Al Taweel, A., & Chen, C. (1996). A Novel Static Mixer for the Effective Dispersion of Immiscible Liquids. *Transactions of the Institution of Chemical Engineers*, *74*, 445-450.
- Al Taweel, A.M., Yan, J., Azizi, F., Odedra, D., & Gomaa, H.G. (2005). Using In-Line Static Mixers to Intensify Gas–Liquid Mass Transfer Processes. *Chemical Engineering Science*, *60*(22), 6378-6390.
- Alzyod, S., Attarakih, M., Hasseine, A., & Bart, H. J. (2017). Steady state modeling of Kühni liquid extraction column using the Spatially Mixed Sectional Quadrature Method of Moments (SM-SQMOM). *Chemical Engineering Research and Design*, *117*, 549-556.
- Amokrane, A., Charton, S., Sheibat-Othman, N., Becker, J., Klein, J.P., & Puel, F. (2014). Development of a CFD–PBE Coupled Model for the Simulation of the Drops Behaviour in a Pulsed Column. *The Canadian Journal of Chemical Engineering*, *92*(2), 220–233.
- Angelidou, C., Psimopoulos, M., & Jameson, G.J. (1979). Size Distribution Functions of Dispersions. *Chemical Engineering Science*, *34*(5), 671-676.

Argyriou, D.T., Harvey, L.L., & Shinnar, R. (1971). Bubble Growth by Coalescence in Gas Fluidized Beds. *AIChE Journal*, 17(1), 122-130.

Azizi, F., & Al Taweel, A.M. (2007). Population Balance Simulation of Gas-Liquid Contacting. *Chemical Engineering Science*, 62, 7436-7445.

Azizi, F., & Al Taweel, A.M. (2010). Algorithm for the Accurate Numerical Solution of PBE for Drop Breakup and Coalescence under High Shear Rates. *Chemical Engineering Science*, 65, 6112-6127.

Azizi, F., & Abou Hweij, K. (2017). Liquid-phase axial dispersion of turbulent gas-liquid co-current flow through screen-type static mixers. *AIChE Journal*, 63(4), 1390-1403.

Batterham, R. J., Hall, J. S., & Barton, G. W. (1981). Pelletizing kinetics and simulation of full scale balling circuits.

Bennani, A., Gence, J.N., & Mathieu, J. (1985). The Influence of a Grid-Generated Turbulence on the Development of Chemical Reactions. *AIChE Journal*, 31(7), 1157-1166.

Bourne, J.R., & Lips, M. (1991). Micromixing in Grid-Generated Turbulence: Theoretical Analysis and Experimental Study. *The Chemical Engineering Journal*, 47(3), 155-162.

Brucato, A., Ciofalo, M., Grisafi, F., & Tocco, R. (2000). On the Simulation of Stirred Tank Reactors via Computational Fluid Dynamics. *Chemical Engineering Science*, 55(2), 291-302.

Buffo, A., Vanni, M., Marchisio, D. L., & Fox, R. O. (2013a). Multivariate quadrature-based moments methods for turbulent polydisperse gas–liquid systems. *International Journal of Multiphase Flow*, *50*, 41-57.

Buffo, A., Marchisio, D.L., Vanni, M., & Renze, P. (2013b). Simulation of polydisperse multiphase systems using population balances and example application to bubbly flows. *Chemical Engineering Research and Design*, *91*, 1859-1875.

Cachaza Gianzo, E.M. (2011). Hydrodynamics and Mass Transfer Effects in Bubble Columns. PhD Thesis, Universidad de Salamanca, Salamanca, Spain.

Chen, Al Taweel, A. (2007). An experimental investigation of gas-liquid contacting in screen-type static mixers.

Chen, P., Sanyal, J., & Duduković, M.P. (2005a). Numerical simulation of bubble columns flows: effect of different breakup and coalescence closures. *Chemical Engineering Science*, *60*(4), 1085-1101.

Chen, P., Duduković, M.P., & Sanyal, J. (2005b). Three-dimensional simulation of bubble column flows with bubble coalescence and breakup. *AIChE Journal*, *51*(3), 696-712.

Chesters, A.K. (1991). Modelling of Coalescence Processes in Fluid-Liquid Dispersions: A Review of Current Understanding. *Transactions of the Institution of Chemical Engineers*, *69*(A), 259-270.

Coulaloglou, C.A., & Tavlarides, L.L. (1977). Description of Interaction Processes in Agitated Liquid-Liquid Dispersions. *Chemical Engineering Science*, *32*, 1289-1297.

Courant, R. (1943). Variational methods for the solution of problems of equilibrium and vibrations. *Bulletin of the American Mathematical Society*, 49, 1-23.

Dafniotis, P. (1996). Modeling of Emulsion Copolymerization Reactors Operating Below the Critical Micelle Concentration, Ph.D. Thesis, University of Wisconsin, Madison, WI.

Deju, L., Cheung, S.C.P., Yeoh, G.H., Qi, F. & Tu, J. (2015). Comparative Analysis of Coalescence and Breakage Kernels in Vertical Gas-Liquid Flow. *The Canadian Journal of Chemical Engineering*, 93(7), 1295-1310.

Diaz, M.E., Iranzo, A., Cuadra, D., Barbero, R., Montes, F.J., & Galan, M.A. (2008a). Numerical Solution of the Gas-Liquid Flow in a Laboratory Scale Bubble Column Influence of Bubble Size Distribution and Non-Drag Forces. *The Chemical Engineering Journal*, 139, 363-379.

Diaz, M.E., Montes, F.J., & Galan, M.A. (2008b). Experimental Study of the Transition Between Unsteady Flow Regimes in a Partially Aerated Two-Dimensional Bubble Column. *Chemical Engineering and Processing*, 47, 1867-1876.

Ding, A., Hounslow, M.J., & Biggs, C.A. (2006). Population balance modelling of activated sludge flocculation: Investigating the size dependence of aggregation, breakage and collision efficiency. *Chemical Engineering Science*, 61(1), 63-74.

Dorao, C. A., & Jakobsen, H. A. (2007). Least-squares spectral method for solving advective population balance problems. *Journal of Computational and Applied Mathematics*, 201(1), 247-257.

- Ekambara, K., Sanders, R. S., Nandakumar, K., & Masliyah, J. H. (2012). CFD modeling of gas-liquid bubbly flow in horizontal pipes: influence of bubble coalescence and breakup. *International Journal of Chemical Engineering*, 2012.
- Galerkin, B. G. (1915). Series solution of some problems of elastic equilibrium of rods and plates. *Vestn. Inzh. Tekh*, 19, 897-908.
- Ganesan, S. (2012). An operator-splitting Galerkin/SUPG finite element method for population balance equations: stability and convergence. *ESAIM: Mathematical Modelling and Numerical Analysis*, 46(6), 1447-1465.
- Guido-Lavalle, G., Carrica, P., & Qazi, M.K. (1994). A Bubble Number Density Constitutive Equation. *Nuclear Engineering and Design*, 152(1-3), 213-224.
- Hagesaether, L., Jakobsen, H.A., & Svendsen, H.F. (2002). A model for turbulent binary breakup of dispersed fluid particles. *Chemical Engineering Science*, 57(16), 3251-3267.
- Harris, C.K., Roekaerts, D., Rosendal, F.J.J., Buitendijk, F.G.J., Daskopoulos, Ph., Vreenegoor, A.J.N., & Wang, H. (1996). Computational Fluid Dynamics for Chemical Reactor Engineering. *Chemical Engineering Science*, 51(10), 1569-1594.
- Herrero, V.A., Guido-Lavalle, G., & Clause, A. (1995). Non-Equilibrium Effects in Void Fraction Distribution. *Nuclear Engineering and Design*, 154(2), 183-192.
- Hesketh, R.P., Etchells, A.W., & Fraser Russel, T.W. (1991). Experimental Observation of Bubble Breakage in Turbulent Flow. *Industrial and Engineering Chemistry Research*, 30(5), 835-841.

- Hounslow, M.J., Ryall, R.L., & Marshall, V.R. (1988). A Discretized Population Balance for Aggregation, Growth, and Nucleation. *AIChE Journal*, 34(11), 1821-2832.
- Hrennikoff, A. (1941). Solution of problems of elasticity by the framework method. *Journal of applied mechanics*. 8(4), 169-175.
- Hsia, A.M, & Tavlarides, L.L. (1983). Simulation Analysis of Drop Breakage, Coalescence, and Micromixing in Liquid-Liquid Stirred Tanks. *The Chemical Engineering Journal*, 26(3), 189-199.
- Hulbert, H.M., & Katz, S. (1964). Some Problems in Particle Technology: A Statistical Mechanical Formulation. *Chemical Engineering Science*, 19(8), 555-574.
- Hweij, K. A., & Azizi, F. (2015). Hydrodynamics and residence time distribution of liquid flow in tubular reactors equipped with screen-type static mixers. *Chemical Engineering Journal*, 279, 948-963.
- Jakobsen, H.A., Lindborg, H., & Dorao, C.A. (2005). Modeling of Bubble Column Reactors: Progress and Limitations. *Industrial and Engineering Chemistry Research*, 44(14), 5107-5151.
- Jairazbhoy, V., & Tavlarides, L.L. (2000). A numerical technique for the solution of integrodifferential equations arising from balances over populations of drops in turbulent flows. *Computers and Chemical Engineering*, 23(11-12), 1725-1735.
- John, V., Mitkova, T., Roland, M., Sundmacher, K., Tobiska, L., & Voigt, A. (2009). Simulations of population balance systems with one internal coordinate using finite element methods. *Chemical Engineering Science*, 64(4), 733-741.

- Jonsson, G., & Palsson, O.P. (1991). Use of Empirical Relations in the Parameters of Heat-Exchanger Models. *Industrial and Engineering Chemistry Research*, 30(6), 1193-1199.
- Joshi, J.B. (2002). Reduction of Empiricism through Flow Visualization and Computational Fluid Dynamics. *Chemical Engineering & Technology*, 25(3), 321–328
- Kálal, Z., Jahoda, M., & Fořt, I. (2014). CFD prediction of gas-liquid flow in an aerated stirred vessel using the population balance model. *Chemical and Process Engineering*, 35(1), 55-73.
- Kim, J., & Kramer, T.A. (2006). Improved orthokinetic coagulation model for fractal colloids: Aggregation and breakup. *Chemical Engineering Science*, 61(1), 45-53.
- Kocamustafaogullari, G., & Ishii, M. (1995). Foundation of the Interfacial Area Transport Equation and its Closure Relations. *International Journal of Heat and Mass Transfer*, 38(3), 481-493.
- Kostoglou, M., & Karabelas, A.J. (1994). Evaluation of Zero Order Methods for Simulating Particle Coagulation. *Journal of Colloid and Interface Science*, 163(2), 420-431.
- Kostoglou, M., & Karabelas, A.J. (1995). Effect of Roughness on Energy of Repulsion between Colloidal Surfaces. *Journal of Colloid and Interface Science*, 171(1), 187-199.
- Kumar, S., & Ramkrishna, D. (1996a). On the solution of population balance equations by discretization—I. A fixed pivot technique. *Chemical Engineering Science*, 51(8), 1311-1332.

- Kumar, S., & Ramkrishna, D. (1996b). On the solution of population balance equations by discretization—II. A moving pivot technique. *Chemical Engineering Science*, 51(8), 1333-1342.
- Kumar, J., Peglow, M., Warnecke, G., Heinrich, S., & Mörl, L. (2006). Improved accuracy and convergence of discretized population balance for aggregation: The cell average technique. *Chemical Engineering Science*, 61(10), 3327-3342.
- Kumar, B. (2009). Variability of Energy Dissipation and Shear Rate with Geometry in Unbaffled Surface Aerator. *Bulletin of Chemical Reaction Engineering & Catalysis*, 4(2), 2009, 55-60.
- Laakkonen, M., Alopaeus, V., & Aittamaa, J. (2006). Validation of bubble breakage, coalescence and mass transfer models for gas–liquid dispersion in agitated vessel. *Chemical Engineering Science*, 61(1), 218-228.
- Laakkonen, M., Moilanen, P., Alopaeus, V., & Aittamaa, J. (2007). Modelling local bubble size distributions in agitated vessels. *Chemical Engineering Science*, 62(3), 721-740.
- Lamont, J.C., & Scott, D.S. (1970). An eddy cell model of mass transfer into the surface of a turbulent liquid. *AIChE Journal*, 16(4), 513-519.
- Lasheras, J.C., Eastwood, C., Martinez-Bazan, C., & Montanes, J.L. (2002). A review of statistical models for the break-up of an immiscible fluid immersed into a fully developed turbulent flow. *International Journal of Multiphase Flow*, 28(2), 247-278.
- Levich, V. G. (1962). *Physicochemical hydrodynamics:(by) veniamin G. Levich. Transl. by scripta technica, inc.* Prentice Hall.

Lehr, F., & Mewes, D. (1999, October). A transport equation for the interfacial area density in two-phase flow. In *Second European Congress of Chemical Engineering, Montpellier, France*.

Lehr, F., & Mewes, D. (2001). A transport equation for the interfacial area density applied to bubble columns. *Chemical Engineering Science*, 56(3), 1159-1166.

Lehr, F., Millies, M., & Mewes, D. (2002). Bubble-Size distributions and flow fields in bubble columns. *AIChE Journal*, 48(11), 2426-2443.

Liao, Y., & Lucas, D. (2009). A literature review of theoretical models for drop and bubble breakup in turbulent dispersions. *Chemical Engineering Science*, 64(15), 3389-3406.

Liao, Y., & Lucas, D. (2010). A Literature Review on Mechanisms and Models for the Coalescence Process of Fluid Particles. *Chemical Engineering Science*, 65, 2851-2864.

Lucas, D., Beyer, M., Szalinski, L., & Schütz, P. (2010). A new database on the evolution of air–water flows along a large vertical pipe. *International Journal of Thermal Sciences*, 49(4), 664-674.

Luo, H., & Svendsen, H.F. (1996). Theoretical Model for Drop and Bubble Breakup in Turbulent Dispersions. *AIChE Journal*, 42(5), 1225-1233.

Luo, H., & Svendsen, H.F. (1996). Modeling and Simulation of Binary Approach by Energy Conservation Analysis. *Chemical Engineering Communications*, 145, 145-153.

Maaß, S., Metz, F., Rehm, T., & Kraume, M. (2010). Prediction of drop sizes for liquid–liquid systems in stirred slim reactors—Part I: Single stage impellers. *Chemical Engineering Journal*, 162(2), 792-801.

Mahoney, A. W., & Ramkrishna, D. (2002). Efficient solution of population balance equations with discontinuities by finite elements. *Chemical Engineering Science*, 57(7), 1107-1119.

Mantzaris, N. V., Daoutidis, P., & Sreenc, F. (2001). Numerical solution of multi-variable cell population balance models. III. Finite element methods. *Computers & Chemical Engineering*, 25(11-12), 1463-1481.

Marchisio, D.L., Piktorna, J.T., Fox, R.O., Vigil, R.D., & Barresi, A.A. (2003). Quadrature Method of Moments for Population-Balance Equations. *AIChE Journal*, 49, 1266-1276.

Martínez-Bazán, C., Lasheras, J. C., & Montañes, J. L. (1998, November). On the break-up of air bubbles in a fully developed turbulent flow. In *APS Division of Fluid Dynamics Meeting Abstracts*.

Martinez-Bazan, C., Montanes, J. L., & Lasheras, J. C. (1999). On the breakup of an air bubble injected into a fully developed turbulent flow. Part 1. Breakup frequency. *Journal of Fluid Mechanics*, 401, 157-182.

Martinez-Bazan, C., Montanes, J. L., & Lasheras, J. C. (1999). On the breakup of an air bubble injected into a fully developed turbulent flow. Part 2. Size PDF of the resulting daughter bubbles. *Journal of Fluid Mechanics*, 401, 183-207.

- Martin-Valdepenas, J. M., Jimenez, M. A., Barbero, R., & Martin-Fuertes, F. (2007). A CFD comparative study of bubble break-up models in a turbulent multiphase jet. *Heat and mass transfer*, 43(8), 787-799.
- Maxey, M.R., & Riley, J.J. (1983). Equation of Motion for a Small Rigid Particle in a Non-Uniform Flow. *Physics of Fluids*, 26, 883-889.
- McGraw, R. (1997). Description of aerosol dynamics by the quadrature method of moments. *Aerosol Science and Technology*, 27(2), 255-265.
- Meimaroglou, D., Roussos, A. I., & Kiparissides, C. (2006). Part IV: Dynamic evolution of the particle size distribution in particulate processes. A comparative study between Monte Carlo and the generalized method of moments. *Chemical Engineering Science*, 61(17), 5620-5635.
- Millies, M., & Mewes, D. (1999). Interfacial Area Density in Bubbly Flow. *Chemical Engineering and Processing: Process Intensification*, 38(4-6), 307-319.
- Narsimhan, G., Gupta, J. P., & Ramkrishna, D. (1979). A model for transitional breakage probability of droplets in agitated lean liquid-liquid dispersions. *Chemical Engineering Science*, 34(2), 257-265.
- Nicmanis, M., & Hounslow, M. J. (1996). A finite element analysis of the steady state population balance equation for particulate systems: Aggregation and growth. *Computers & chemical engineering*, 20, S261-S266.
- Orszag, S. A. (1969). Numerical methods for the simulation of turbulence. *The Physics of Fluids*, 12(12), II-250.

- Oshinowo, L., & Kuhn, D.C.S. (2000). Turbulence Decay behind Expanded Metal Screens. *The Canadian Journal of Chemical Engineering*, 78(6), 1032-1039.
- Petitti, M., Nasuti, A., Marchisio, D. L., Vanni, M., Baldi, G., Mancini, N., & Podenzani, F. (2010). Bubble size distribution modeling in stirred gas–liquid reactors with QMOM augmented by a new correction algorithm. *AIChE Journal*, 56(1), 36-53.
- Pfleger, D., Gomes, S., Gilbert, N., & Wagner, H. G. (1999). Hydrodynamic simulations of laboratory scale bubble columns fundamental studies of the Eulerian–Eulerian modelling approach. *Chemical Engineering Science*, 54(21), 5091-5099.
- Prince, M.J., & Blanch, H.W. (1990). Bubble Coalescence and Breakup in Air-Sparged Bubble Column. *AIChE Journal*, 36(10), 1485-1499.
- Ramkrishna, D. (1981). Analysis of population balance—IV: The precise connection between Monte Carlo simulation and population balances. *Chemical Engineering Science*, 36(7), 1203-1209.
- Ramkrishna, D. (1985). Status of Population Balances. *Reviews in Chemical Engineering*, 3, 49-95.
- Ramkrishna, D., & Singh, M.R. (2014). Population Balance Modeling: Current Status and Future Prospects. *Annual Review of Chemical and Biomolecular Engineering*, 5, 123-146.
- Randolph, A.D. (1964). A Population Balance for Countable Entities. *The Canadian Journal of Chemical Engineering*, 42(6), 280-281.

- Rao, A., Sathe, M., Reddy, R.K., & Nandakumar, K. (2016). CFD with Population Balance Model to Predict Droplet Size Distribution in Submerged Turbulent Multiphase Jets. *The Canadian Journal of Chemical Engineering*, 94(11), 2072–2085.
- Rauline, D., Tanguy, P.A., Le Blévec, J.-M., & Bousquet, J. (1998). Numerical Investigation of the Performance of Several Static Mixers. *The Canadian Journal of Chemical Engineering*, 76, 527-535.
- Rauline, D., Le Blévec, J.-M., Bousquet, J., & Tanguy, P.A. (2000). A Comparative Assessment of the Performance of the Kenics and SMX Static Mixers. *Trans IChemE*, 78(A), 389-396.
- Razzaghi, K., & Shahraki, F. (2016). Theoretical Model for Multiple Breakup of Fluid Particles in Turbulent Flow Field. *AIChE Journal*, 62(12), 4508-4525.
- Rigopoulos, S. (2010). Population balance modelling of polydispersed particles in reactive flows. *Progress in Energy and Combustion Science*, 36(4), 412-443.
- Saliakas, V., Kotoulas, C., Meimaroglou, D., & Kiparissides, C. (2008). Dynamic Evolution of the Particle Size Distribution in Suspension Polymerization Reactors: A Comparative Study on Monte Carlo and Sectional Grid Methods. *The Canadian Journal of Chemical Engineering*, 86, 924-936.
- Sahu, A.K., Kumar, P., Patwardhan, A.W., & Joshi, J.B. (1999). CFD Modelling and Mixing in Stirred Tanks. *Chemical Engineering Science*, 54(13-14), 2285-2293.
- Schmidt, S.A., Simon, M., Attarakih, M.M., Lagar, G.L., & Bart, H.J. (2006). Droplet population balance modelling—hydrodynamics and mass transfer. *Chemical Engineering Science*, 61(1), 246-256.

- Shah, B.H., Ramkrishna, D., & Borwanker, J.D. (1977). Simulation of particulate systems using the concept of the interval of quiescence. *AIChE Journal*, 23(6), 897-904.
- Singh, R., & Kumar, S. (2006). Effect of mixing on nanoparticle formation in micellar route. *Chemical engineering science*, 61(1), 192-204.
- Solsvik, J., Tangen, S., & Jakobsen, H. A. (2013). On the constitutive equations for fluid particle breakage. *Reviews in Chemical Engineering*, 29(5), 241-356.
- Solsvik, J., & Jakobsen, H. A. (2015). Single air bubble breakup experiments in stirred water tank. *International Journal of Chemical Reactor Engineering*, 13(4), 477-491.
- Solsvik, J., & Jakobsen, H. A. (2016). Spectral solution of the breakage–coalescence population balance equation Picard and Newton iteration methods. *Applied Mathematical Modelling*, 40(3), 1741-1753.
- Solsvik, J., Skjervold, V. T., & Jakobsen, H. A. (2017). A bubble breakage model for finite Reynolds number flows. *Journal of Dispersion Science and Technology*, 38(7), 973-978.
- Sommer, M., Stenger, F., Peukert, W., & Wagner, N.J. (2006). Agglomeration and breakage of nanoparticles in stirred media mills—a comparison of different methods and models. *Chemical Engineering Science*, 61(1), 135-148.
- Sommerfeld, M., & Decker, S. (2004). State of the Art and Future Trends in CFD Simulation of Stirred Vessel Hydrodynamics. *Chemical Engineering & Technology*, 27(3), 215–224.

- Spielman, L.A., & Levenspiel, O. (1965). A Monte Carlo treatment for reacting and coalescing dispersed phase systems. *Chemical Engineering Science*, 20(3), 247-254.
- Thakur, R.K., Vial, Ch., Nigam, K.D.P., Nauman, E.B., & Djelveh, G. (2003). Static Mixers in the Process Industries—A Review. *Chemical Engineering Research and Design*, 81(7), 787-826.
- Tsouris, C., & Tavlarides, L.L. (1994). Breakage and Coalescence Models for Drops in Turbulent Dispersions. *AIChE Journal*, 40(3), 395-406.
- Wang, T., Wang, J., & Jin, Y. (2003). A Novel Theoretical Breakup Kernel Function for Bubbles/Droplets in a Turbulent Flow. *Chemical Engineering Science*, 58, 4629-4637.
- Wang, T., Wang, J., & Jin, J. (2004). An Efficient Numerical Algorithm for "A Novel Theoretical Breakup Kernel Function for Bubbles/Droplets in a Turbulent Flow". *Chemical Engineering Science*, 59, 2593-2595.
- Wang, T., Wang, J., & Jin, Y. (2005a). Theoretical Prediction of Flow Regime Transition in Bubble Columns by the Population Balance Model. *Chemical Engineering Science*, 60, 6199-6209.
- Wang, T., Wang, J., & Jin, Y. (2005b). Population Balance Model for Gas-Liquid Flows: Influence of Bubble Coalescence and Breakup Models. *Industrial and Engineering Chemistry Research*, 44, 7540-7549.
- Xing, C., Wang, T., Guo, K., & Wang, J. (2014). A Unified Theoretical Model for Breakup of Bubbles and Droplets in Turbulent Flows. *AIChE Journal*, 61(4), 1391-1403.

Zaccone, A., Gäbler, A., Maaß, S., Marchisio, D., & Kraume, M. (2007). Drop breakage in liquid-liquid stirred dispersions: modelling of single drop breakage. *Chemical Engineering Science*, *62*, 6297-6307.

Ziókowski, D., & Morawski, J. (1987). The Flow Characteristic of the Liquid Streams inside a Tubular Apparatus Equipped with Static Mixing Elements of a New Type. *Chemical Engineering and Processing: Process Intensification*, *21*(3), 131-139.

Zhang, N., Calabrese, R.V., & Gentry, J.W. (1992). Fundamental properties of interlaced fibonacci sequences and their potential in describing particle breakage. *Journal of Aerosol Science*, *23*(Supplement 1), 193-196.

Zhan, S., Wang, J., Wang, Z., & Yang, J. (2018). Computational Fluid Dynamics-Population Balance Model Simulation of Effects of Cell Design and Operating Parameters on Gas-Liquid Two-Phase Flows and Bubble Distribution Characteristics in Aluminum Electrolysis Cell. *Technical Communications*, *70*(2), 229-236.

Zhao, H., & Ge, W. (2007). A theoretical bubble breakup model for slurry beds or three-phase fluidized beds under high pressure. *Chemical Engineering Science*, *62*(1-2), 109-115.